Author:
Exley, Ben

Title:
The role of the nucleus reuniens of the thalamus in the recognition memory network

The role of the nucleus reuniens of the thalamus in the recognition memory network

Benjamin Matthew Stuart Exley

A dissertation submitted to the University of Bristol in accordance with the requirements for award of the degree of Master by Research in the Faculty of Life Sciences.

School of Physiology, Pharmacology and Neuroscience, April 2019

Word count: 13,689

Abstract

Recognition memory provides the ability to judge if a stimulus has been encountered before. Depending on the type of information to be used for recognition, this process depends on a functional interaction between several brain regions including perirhinal cortex, hippocampus and medial prefrontal cortex. Recent studies have also implicated the nucleus reuniens of the thalamus (NRe) in recognition memory tasks with a high mnemonic demand, possibly by facilitating information flow between hippocampus and medial prefrontal cortex. Using Bayesian hierarchical modelling, the present study investigated if the NRe modulates neural activity within the recognition memory network.

Recognition memory of rats with a lesion in the NRe was compared to rats which received a sham surgery. Recognition memory was tested using a bow-tie maze task, in which rats explored either novel or highly familiar objects across a number of training sessions. Expression of the immediate early gene c-fos, a marker for neuronal activation, was measured in selected brain regions by immunohistochemistry. Levels of Fos-positive nuclei were assessed in the four experimental groups (Sham-Novel, Sham-Familiar, Lesion-Novel, Lesion-Familiar) using both standard frequentist statistics and Bayesian modelling. Analysis of object discrimination demonstrated that lesions in the NRe did not affect recognition memory performance and confirmed that both Sham-Familiar and Lesion-Familiar rats had encoded and recognised the repeatedly presented objects. Bayesian modelling outperformed frequentist statistics by estimating means with higher accuracy and reduced uncertainty. According to the Bayesian model, NRe lesions significantly affected Fos levels in the perirhinal cortex, TE2, dorsal peduncular cortex, CA3, dentate gyrus and subiculum.

The results suggest that the absence of the NRe alters neural activity in the recognition memory network when rats explore novel or familiar objects and presumably encode stimulus and associative information. While the precise role of the NRe in recognition memory remains to be defined, the present study supports the hypothesis that the NRe modulates information flow within the recognition memory network.

Acknowledgements

First and foremost, I would like to acknowledge and thank my supervisors, Prof Clea Warburton and Dr Cian O'Donnell for their guidance, belief and support throughout the project. Additionally, I would like to thank my academic progress assessors, Prof Elek Molnár and Dr Peter Brennan who provided sound feedback and advice throughout the initial stages of the project.

I would also like to convey my appreciation to the members of the Bashir/Warburton group especially Dr Gareth Barker for training me in surgery and in the laboratory and for having a wealth of information that he was always glad to share, and Dr Clair Booth for assisting me in my behavioural and lab experiments when timing was a factor. I would also like to give thanks to both Dr Booth and Dr Silviu Rusu for providing me with some useful self-developed software which served to considerably shorten the analysis time of my experiments.

Last but not least, I would like to thank the members of the Wolfson Bioimaging Facility, in particular Dr Stephen Cross, for his tireless help, collaboration and support during the analysis aspect of the project. His knowledge of microscopy and bioimaging analysis was greatly appreciated.

Author’s declaration

I declare that the work in this dissertation was carried out in accordance with the requirements of the University's Regulations and Code of Practice for Research Degree Programmes and that it has not been submitted for any other academic award. Except where indicated by specific reference in the text, the work is the candidate's own work. Work done in collaboration with, or with the assistance of, others, is indicated as such. Any views expressed in the dissertation are those of the author.

SIGNED: .....Benjamin Exley..... DATE: ....22/10/2019....

Table of contents

List of Tables

List of Figures

1. Introduction

Recognition memory allows us to judge if we have encountered something before. The discrimination of a novel from a familiar stimulus, is referred to as 'familiarity discrimination' or 'single-item recognition memory' and requires an intact perirhinal cortex (Ennaceur *et al*., 1996; Bussey *et al*., 1999; Wan *et al*., 1999; Barker *et al*., 2007; Barker and Warburton, 2011). Associative recognition memory, the recognition of a stimulus with memory of additional information of the previous encounter of a stimulus, such as spatial or contextual information, also requires the perirhinal cortex (Bussey *et al*., 2001; Barker *et al*., 2007). In addition, the hippocampus (Barker and Warburton, 2011) and medial prefrontal cortex have been shown to be involved in this type of recognition memory (Mitchell and Laiacona, 1998; Hannesson *et al*, 2004; Barker *et al*., 2007). Moreover, disconnection studies in rats, whereby two of these regions were lesioned unilaterally, produced impairment in associative recognition memory tasks only if the lesions were placed in opposite hemispheres. This suggests that disruption of the functional interaction between the two regions in both hemispheres (Barker *et al*., 2007; Barker and Warburton, 2011) impairs associative recognition memory performance.

1.1. Recognition memory 'circuit'

The observation that associative recognition memory relies on a circuit involving the perirhinal cortex, hippocampus and medial prefrontal cortex, has been further confirmed through experiments in which the specific inactivation of neural pathways between these regions, led to impairment in associative recognition memory tasks (Barker *et al*., 2017).

The presence of a recognition memory circuit has further been studied by measuring the level of neural activity within the network, following a recognition memory task. In these studies, recognition memory was assessed using a bow tie maze procedure developed by Aggleton and colleagues (Albasser *et al*., 2010). The 'bow-tie maze' is a recognition memory task, in which rats are exposed to repeated tests of familiarity discrimination over the course of each training session. Thus, two groups of rats are exposed to one of two different sets of stimuli; group 'Familiar' is exposed to the same set of objects over several training sessions, so that these objects became highly familiar and in the final test session, the rats no longer show discrimination between the object pairs. In contrast, group 'Novel' is shown novel objects throughout the training period, and in the test session. This procedure therefore allows a comparison of neural activity in different brain regions between rats exposed to novel and rats exposed to highly familiar objects (Albasser *et al*., 2010).

1.1.1. Mapping the recognition memory circuit using immediate early gene c-fos

To compare brain-wide neural activation patterns the protein product of the immediate early genes, such as c-fos, can be quantified. c-fos is widely expressed in a number of brain regions, shows low constitutive expression under basal conditions and is expressed rapidly following neuronal stimulation, peaking at 90 minutes following exposure to the stimulus; thus, it can be used as a measure of neuronal activity (Morgan *et al*., 1987; Bullitt, 1990). The c-fos gene codes for the protein Fos, a transcription factor that goes on to induce expression of downstream late response genes, known to influence neuronal physiology.

Previous studies have demonstrated higher protein levels of Fos in the perirhinal cortex following exposure to a novel stimulus, compared to a familiar stimulus (Zhu *et al*., 1995b; Zhu *et al*., 1996; Wan *et al*., 1999), mirroring the increased neuronal responses observed in rats exposed to novel versus familiar objects (Zhu *et al*., 1995a). Therefore, c-fos expression in the perirhinal cortex is suitable as a marker of neuronal activity during recognition memory formation.

Use of c-fos as an activity marker is not without its limitations; c-fos expression lacks temporal resolution, it does not always correlate with neural activation or result in long-term changes in gene expression and since c-fos expression is induced by a variety of stimuli, it cannot be identified with certainty which stimulus activated the neuron (Kovács, 2008).

Despite these drawbacks, c-fos provides a simple and sensitive marker of neuronal activity that has been used successfully to map out neural pathways that are activated by specific stimuli. Albasser *et al*. used a statistical modelling approach to study the correlation of Fos levels in the different brain regions to produce a model of information flow within the network following exposure to either novel or familiar stimuli (Albasser *et al*., 2010) (Figure 1.1). While following exposure to both novel and familiar stimuli, the information required for recognition memory formation appeared to flow from the perirhinal cortex via the entorhinal cortex to the hippocampus, importantly the pathway by which the novel or familiar passed through the circuit differed. Thus, exposure to novel stimuli appeared to engage a route from the entorhinal cortex to the hippocampus via the perforant path, while following exposure to familiar objects the temporo-ammonic pathway was preferred.

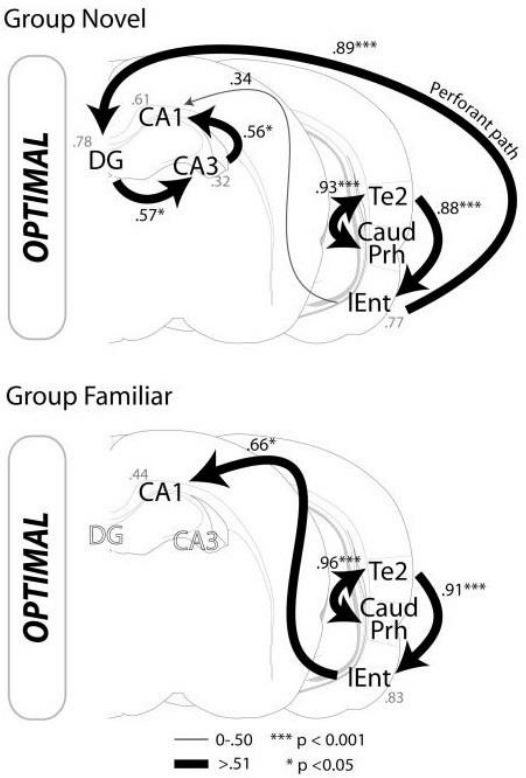

Figure 1.1: Information flow within the memory network following exposure to novel (top) or familiar stimuli (bottom). Caud Prh, caudal perirhinal cortex. DG, dentate gyrus. lEnt, lateral entorhinal cortex. Te2, temporal association cortex. Adapted from Albasser et al 2010.

1.2. Nucleus Reuniens

Recently, the nucleus reuniens of the thalamus (NRe) has been suggested as a further component of the recognition memory circuit (Barker and Warburton, 2018). The NRe is the largest of the midline thalamic nuclei and is located along the entire rostral-caudal extent of the thalamus. In terms of understanding the neural mechanisms of recognition memory, the NRe is of particular interest due to its many anatomical connections to both cortical and sub-cortical regions of the brain (Vertes, 2002; McKenna and Vertes, 2004; Vertes *et al*., 2006; Hoover and Vertes, 2012; Mathiasen *et al*., 2019). Specifically, it is connected to several of the brain regions that are considered to form the recognition memory network (Figure 1.2).

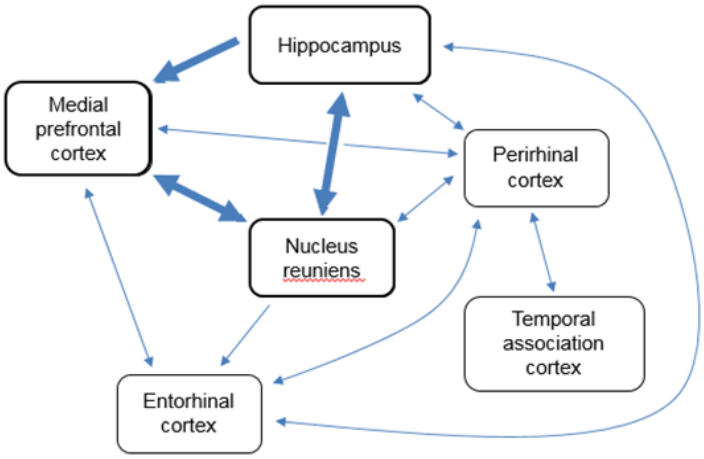

Figure 1.2: Diagram of the anatomical connections of the recognition memory network. The potential sub-circuit with the nucleus reuniens as a relay point between hippocampus and medial prefrontal cortex is highlighted in bold

Anatomical studies therefore indicate that the NRe has the potential to act as a relay point between medial prefrontal cortex and hippocampus; it shares bidirectional connections with both regions, whereas there is only a direct connection from the hippocampus to the medial prefrontal cortex, but not in the opposite direction (Vertes, 2002; Hoover and Vertes, 2012). In addition, the NRe is bidirectionally connected to the perirhinal cortex (PRh), which as previously stated, plays a central role in familiarity discrimination and associative recognition memory (McKenna and Vertes, 2004; Vertes *et al*., 2006).

A number of studies have explored the role of the NRe in memory in the context of spatial memory. Inactivation of the NRe (N.B. the neighbouring rhomboid nucleus is often also affected) did not impair acquisition of hippocampal-dependent spatial memory, assessed in the Morris water maze task (Cholvin *et al*., 2013; Dolleman-van der Weel *et al*., 2009; Lourerio *et al*., 2012). However, NRe lesioned rats were found to use a different strategy to navigate to the platform, compared to a control group (Dolleman-van der Weel *et al*., 2009). A similar

observation was made in an experiment using a double-H shaped water maze. In this task the rats had to learn the route to a platform and in the probe trial, the rats had to find the platform based on the spatial memory of its location rather than the route. This shifting in behavioural strategy was found to be sensitive to combined inactivation of NRe and rhomboid nucleus (NRh) (Cholvin *et al*., 2013). The combination of spatial memory and behavioural flexibility has previously been shown to require the engagement of both hippocampus and medial prefrontal cortex, and most likely the functional interaction between these two regions. Therefore, it has been suggested that the NRe is involved when information needs to be relayed between these two regions.

The hypothesis that the NRe is only critical in tasks that involve a functional interaction between hippocampus and medial prefrontal cortex, has further been supported by other spatial working memory tasks that require both regions (Hembrook and Mair, 2011; Hembrook *et al*., 2012; Layfield *et al*., 2015 Viena *et al*., 2017). Inactivation of NRe or NRe/NRh has been shown to cause an impairment in a spatial win-shift task, and in a delayed alternation task, in which rats had to visit the arm or arms of a maze they had not previously visited. In one version of this task, if the rats made a wrong choice, they were able to make up to 10 correction runs. Rats with inactivation of the NRe produced a higher number of incorrect choices, suggesting impaired behavioural flexibility (Viena *et al*., 2017). In another working memory task, where the rat had to learn an association between the texture/visual appearance of the floor with the location of a food reward in a T-maze, inactivation of the NRe/NRh impaired performance. As with the tasks described previously, this task relies on both medial prefrontal cortex and hippocampus (Halock *et al*., 2013). In contrast, when rats were tested on a purely hippocampal-dependent, varying choice delayed nonmatching task, NRe/NRh inactivation had no effect (Hembrook *et al*., 2012).

Further experimental evidence has also suggested that the NRe (and NRh) may be important for the consolidation of remote spatial memories. Combined inactivation of these thalamic nuclei impaired retrieval of the platform location at a 25-d delay but not at a 5-d delay. Similarly, increased neural activation was observed within the NRe/NRh only at the long (25-d) delay (Loureiro *et al*., 2012). The retrieval of remote memories is also thought to require a functional interaction of the hippocampus and cortical structures (Lopez *et al*., 2011).

In addition to spatial memory, the contribution of the NRe has also been investigated in fear memory paradigms (Xu and Sudhof, 2013). Mice in which the NRe had been inactivated were able to form contextual fear memories, they also showed freezing behaviour in unconditioned contexts. Thus, the authors hypothesised that the NRe may not be required for fear memory formation per se, instead it might play a role in regulating fear memory generalisation (Xu and Sudhof 2013).

Due to the importance of the functional interaction between the hippocampus and the medial prefrontal cortex in certain types of associative recognition memory and the role of the NRe as a potential relay point between these two structures, Warburton and colleagues recently investigated the role of the NRe in different types of recognition memory (Barker and Warburton, 2018). In this study, inactivation of NRe had no effect on memory performance of either a spontaneous object recognition task or of an object location task (Barker and Warburton, 2018), a task which relies on the hippocampus (Barker and Warburton, 2011). In contrast, disruption of the NRe impaired the encoding and retrieval of long-term associative

recognition memory, as assessed using an object-in-place task (Barker and Warburton, 2018). Interestingly, inhibition of protein synthesis in the NRe also impaired performance in the object-in-place task (Barker and Warburton, 2018). Thus, the NRe seems to play a key functional role within the network for associative recognition memory, rather than simply acting as a relay point.

These previous studies suggest that while the NRe may not be directly involved in the formation of memories that rely on single structures such as the hippocampus (Barker and Warburton, 2018; Cholvin *et al*., 2013; Dolleman-van der Weel *et al*., 2009; Hembrook *et al*., 2012; Lourerio *et al*., 2012), it may be critically involved under certain conditions when (1) the task requires both the hippocampus and the medial prefrontal cortex, and therefore the NRe may facilitate information flow between these two structures, (2) the task has a high cognitive/mnemonic demand or (3) the task involves executive functions, such as behavioural flexibility. How the NRe contributes to memory, and the recognition memory network specifically, is unclear and is the focus of this study.

1.3. Bayesian modelling

Bayesian statistics is a standard statistical framework for analysing and modelling data. Statistical analysis of experimental data is required to make sense of and draw conclusions from experiments, by estimating parameters that are measured in an experiment, for example the ‘true mean’ of a population.

The traditional frequentist approach to statistics calculates the sample mean of the measured data as the most likely estimation of the true mean. In contrast, the Bayesian approach (Figure 1.3) combines prior knowledge (so called ‘prior beliefs’) with the collected data (‘evidence’) to compute a posterior probability distribution from which the parameter estimates (for example, the estimate of the ‘true mean’) is derived (‘posterior beliefs’).

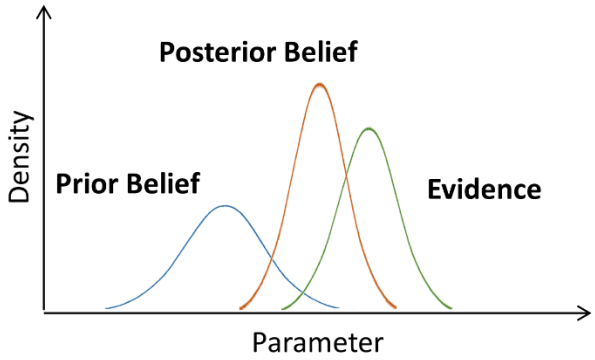

Figure 1.3: Schematic of the Bayesian statistical framework. Bayesian analysis combines the probability distribution describing our prior belief or hypothesis with evidence measured in an experiment, to calculate a posterior probability distribution (posterior beliefs). The posterior distribution describes an updated hypothesis taking into account both the measured data (evidence) and prior beliefs, providing estimates of the true parameters, such as the true mean of the measured data.

Prior distributions guide our expectations of what values the parameters should have, based on observations from previous experiments or on common-sense expectations (for example, gene expression levels cannot be negative). Priors can range from uninformative to highly informative (Figure 1.4). The more informative the defined prior, the more it ultimately contributes to the posterior distribution.

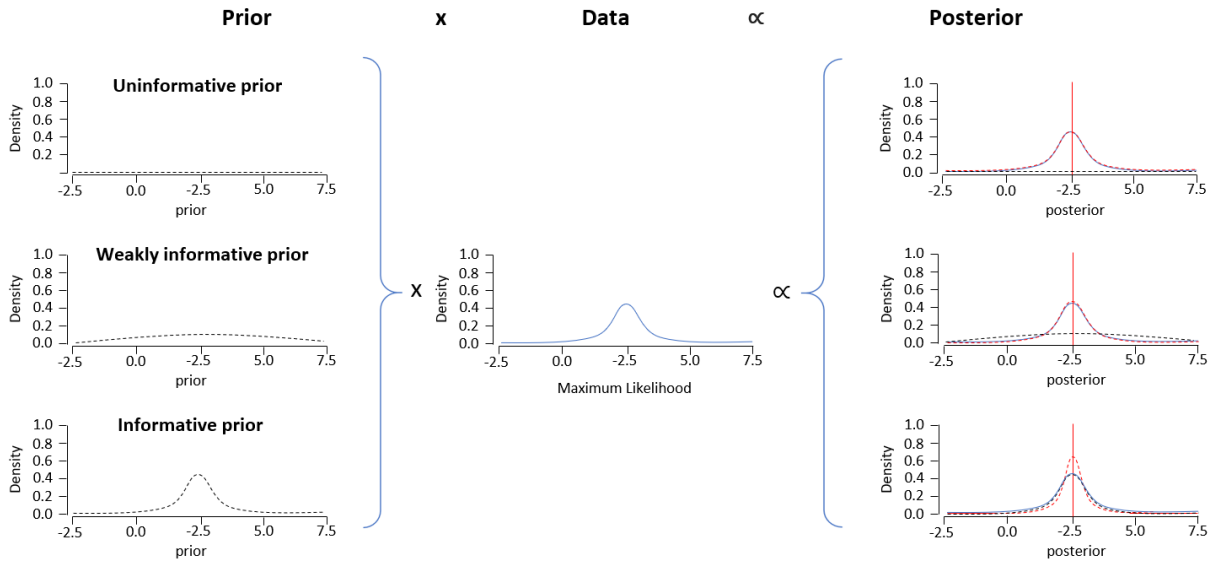

Figure 1.4: Effect of different prior distribution on the posterior distribution. The prior distribution (left) is combined with the data (likelihood function, centre) to obtain the posterior distribution. Uninformative priors barely influence the posterior distribution, while informative priors contribute to the posterior probability distribution to a much greater extent. The solid blue line represents the data in the form of the maximum likelihood. Dashed red line represents posterior probability. Diagram adapted from Van de Schoot & Depaoli, 2014.

The natural and logical way of combining prior information with new data, as is key to the Bayesian approach, fundamentally describes the scientific process; hypotheses are built upon previously acquired knowledge and updated with new knowledge (Kording, 2014).

1.4. Bayesian Probability

Bayesian statistics at its core relies on Bayes' Theorem, which is used to describe conditional probability, i.e. the probability of an event A occurring, given an event B.

The probability of two events A and B occurring, when the two events are not independent from each other, is calculated as the probability of event A occurring given B, multiplied by the probability of B occurring:

$$P(A,B) = P(A|B) * P(B)$$

Equation 1.1

Alternatively, the probability of A and B occurring can also be calculated as the probability of event B given that A occurs, multiplied by the probability of A:

$$P(A,B) = P(B|A) * P(A)$$

Equation 1.2

Setting Equations 1.1 and 1.2 equal to each other, leads to Equation 1.3 shown below:

$$P(A|B) * P(B) = P(B|A) * P(A)$$

Equation 1.3

Dividing Equation 1.3 by the probability of B, leads to Bayes' Theorem:

$$P(A|B) = \frac{P(B|A) * P(A)}{P(B)}$$

Equation 1.4 – Bayes' Theorem

Applying Bayes' theorem to statistical analysis of an experiment allows us to calculate the posterior probability of an estimated parameter (θ), given the observed data (D) from an experiment. The posterior probability is calculated as the probability of the data given the parameter (which is called the 'likelihood'), multiplied by the prior probability of the parameter (the 'prior'), and divided by the probability of the data (or 'evidence').

$$P(\theta|D) = \frac{P(D|\theta) * P(\theta)}{P(D)}$$

Equation 1.5 – Posterior probability

If we consider the posterior parameters as our updated hypothesis, Bayesian statistics enables us to determine the probability that this hypothesis is true. Crucially, in Bayesian modelling, the calculated probabilities are described by distributions, rather than individual values, thereby

providing information regarding the uncertainty associated with the model, as described in the spread or standard deviation of the distribution.

1.5. Advantages of Bayesian statistics

Bayesian statistics has multiple advantages and it mitigates several limitations associated with the frequentist approach. The use of prior information helps reduce uncertainty in a model. It can also reduce the data needed by simplifying future experiments, especially when working with complex datasets involving high-dimensional data, i.e. many parameters that need to be estimated (Kording, 2014).

In addition to the inclusion of prior knowledge, the Bayesian approach is defined by producing a probability distribution for the estimated parameter. This posterior probability distribution quantifies the probability for all possible values of the estimated parameter, rather than the 'most likely' estimate as is the case with frequentist statistics. This negates the need for corrections for multiple testing that are required when using frequentist statistics to reduce the number of false positives (however, that correction in itself, often leads to an increase in the number of false negatives) (Gershman, 2013). The probability distribution further captures the uncertainty associated with the possible values of the estimated parameter, which is important because any model provides only estimates and not definitive values. Therefore, including measures of uncertainty provides information on how correct the estimates are likely to be and enables more accurate interpretation of the results.

Using Bayesian statistics to model data also enables inclusion of the hierarchical structure of the experimental data, e.g. experimental groups, into the analysis model itself (Figure 1.5). A so-called 'hyper-prior' can be defined over a set of parameters. For example, a group-level distribution can be introduced at the level of an experimental group that describes the parameters at the individual level (for example, individual rats within each experimental group) and a global distribution can be computed that describes all the group-level parameters.

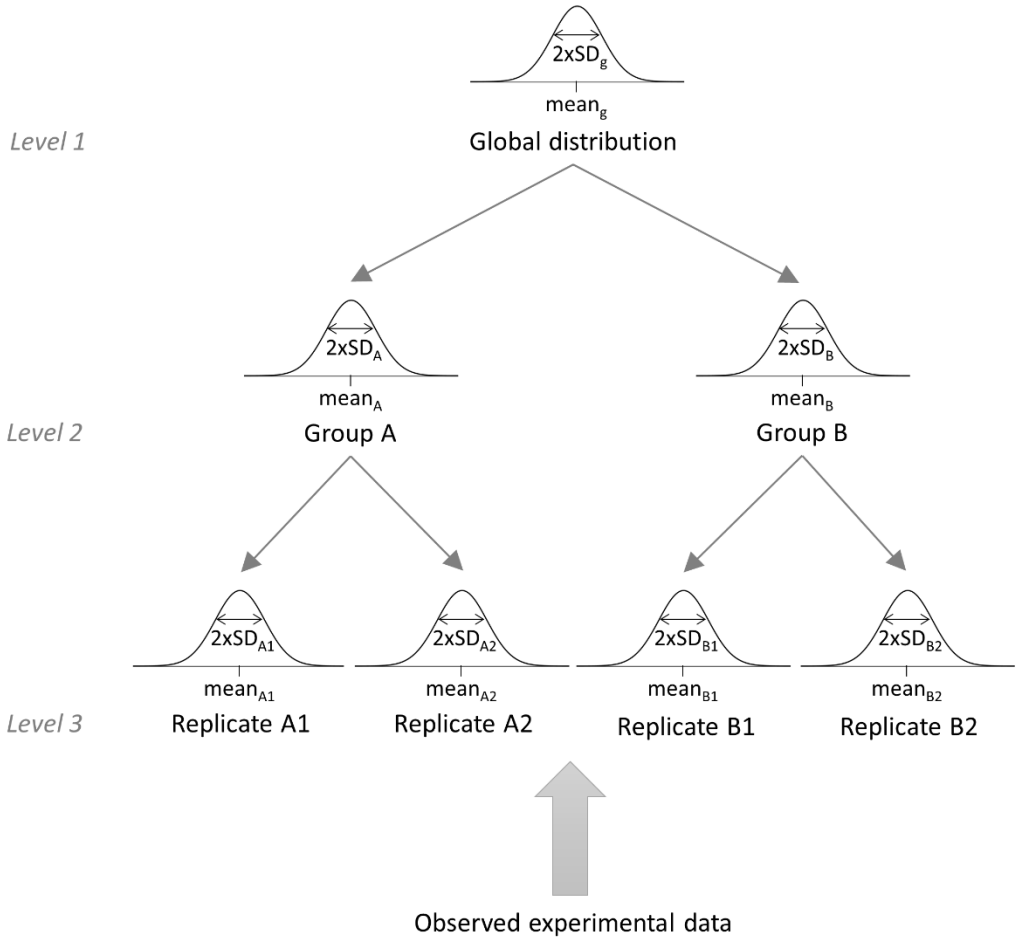

Figure 1.5: Hierarchical model. The Bayesian framework supports inclusion of the hierarchical structure of the experimental data. In this example, data from each replicate is modelled by an individual distribution, defined by a mean and a standard deviation (SD) (Level 3 of the hierarchy). On Level 2 of the hierarchy, replicates are combined into experimental groups, which are governed by one distribution per group, with a respective group mean and standard deviation. These group-level distributions can be described by one global distribution with a global mean and a global standard deviation (Level 1 of the hierarchy, SD_g).

The use of a hyper-prior means that the parameter estimates for one individual are informed by the parameter estimates for the other individuals. As the different individual-level distributions are still retained, this approach is referred to as ‘partial pooling’; an intermediate stage between complete pooling of data, where information on the individual level is not preserved, and complete independence of each individual data point. By assuming that individual values are not completely independent of each other, the whole of the data can be leveraged to make individual estimates more accurate by pulling these individual estimates towards the group mean. The method can mitigate the over-estimation of effect sizes, sometimes observed when using frequentist statistics, and it further strengthens estimates derived from limited data, be it a low number of replicates or missing data.

Fitting the Bayesian model allows us to ask what parameter values are most likely to be consistent with the observed data. In addition, we can use the model parameters to explore post-hoc questions to identify what data should be expected, given the posterior predictive distribution derived from the fitted model. For example, a Bayesian model of the recognition memory network would allow us to manipulate parameters to model lesioning of a specific brain region within the network and subsequent sampling of data from this model. Thus, the derived Bayesian model can be used to generate quantitative predictions to drive future wet-lab experiments.

1.6. Using Bayesian statistics to explore the recognition memory network

Experiments that involve measuring neural activity in brain regions of the recognition memory network (by measuring expression levels of immediate early gene c-fos, for example) come with several limitations. Animal experiments in general tend to be costly, time consuming and need to be planned ethically in accordance with the 3Rs, Replacement, Reduction and Refinement (Russel and Burch, 1959; Prescott and Lidster, 2017), limiting the number of replicates in these experiments. Furthermore, high levels of variability tend to be observed between animals. Bayesian modelling can mitigate these problems by modelling data from a low number of replicates and by reducing and describing the uncertainty associated with the model. The ability to incorporate the hierarchical structure of the data into the analysis, is a further key advantage of the Bayesian approach. Where standard frequentist analysis commonly assumes independence of data, Bayesian analysis allows us to account for, and explicitly model correlations between brain regions that we know exist. Furthermore, the concept of the Bayesian model that can be updated as new data is obtained, enables re-use of data from previous experiments.

In general, implementation of Bayesian statistics takes longer and requires more effort than using standard frequentist methods. Computational tools need to be available that enable running the model fit efficiently. However, as the field of neuroscience and its associated technologies are evolving, larger and more complex information is collected. Statistical analysis needs to be adjusted to deal with these large-scale datasets (Bzdok And Yeo, 2017). Bayesian statistical methods have been extensively applied in the neuroimaging field (e.g. Friston *et al*., 2002, Woolrich, 2012) and other further studies have used Bayesian statistics to model how sensory neurons encode environmental stimuli (Park and Pillow, 2011; Darlington *et al*., 2018). Additionally, other studies have developed Bayesian statistics tools to analyse gene expression in cells (Townsend and Hartl, 2002), including in primary neurons (Gomez-Shiavon *et al*.,2017). McGuinness and colleagues used a Bayesian hierarchical model to estimate amplitudes of and

probabilities associated with Ca^{2+} transients via NMDA receptors in presynaptic boutons of Schaffer collaterals in the hippocampus (McGuinness *et al*., 2010). Despite its clear benefits, so far Bayesian modelling, as an alternative to traditional frequentist statistics, has been under-used in the field of neuroscience.

1.7. Aim of the project

The NRe has been implicated as a key node in a recognition memory network, yet its role is not well understood. In the present study c-fos expression studies are combined with behavioural experimentation, to elucidate specific contributions of the NRe to the information flow within the memory network in a recognition memory task. Therefore, the aim of the project overall is to (1) understand whether NRe modulates neural activation in other nodes of the memory network and (2) develop a statistical model based on Bayesian modelling of information flow within the memory network with and without functional contribution of the NRe, when rats encounter novel or familiar stimuli.

2. Materials and Methods

2.1. Rat surgery and behavioural experimentation

Male Lister Hooded rats (Envigo, UK) with weights ranging from 350 – 450 grams were used for all experiments. All animal procedures were performed in accordance with United Kingdom Animal Scientific Procedures Act (1986) and associated guidelines. All efforts were made to minimise any suffering and the number of animals used.

Experimental Design

The experiment consisted of six cohorts with a total of 40 rats used, giving an experimental group number of 10. The first two cohorts (CO-01 and CO-02) consisted of four rats per cohort and cohorts three to six (CO-03-CO-06) consisted of eight rats per cohort. All rats underwent surgery and subsequent behavioural testing. Rats were kept four per cage on a reversed 12hr light/dark cycle (dark from 08:00 – 20:00, light from 20:00 – 08:00), with behavioural testing taking place during the dark phase, when the rats show higher levels of activity. Food and water was available *ad libitum* until two days before behavioural testing, when all rats within the behavioural cohort were placed on food restriction. The rats were weighed prior to the start of food restriction, to establish a base weight. Following commencement of food restriction, the rats were routinely weighed on a daily basis to ensure they didn't fall below 85% of their original weight. Water was available *ad libitum* throughout the food restriction period and food was provided for 2 hours per day, between 17:00 and 19:00.

If any of the rats fell below 85% of their original weight, the Named Animal Care and Welfare Officer (NACWO) would be informed, along with the resident veterinary surgeon if deemed necessary. The animal would be provided with additional food. If the weight of the animal had not risen above 85% of its base-weight, within a 24hr period, it would subsequently be removed from the experiment. None of the rats' weights fell below 90% of their original weight throughout each experiment.

2.2. Surgery

For cohorts CO-01 and CO-02, two rats received lesions in the NRe and two rats underwent sham surgery. In cohorts CO-03 - CO-06, four rats received lesions in the NRe and four underwent sham surgery. Rats were weighed prior to surgery. For both the lesion and sham groups, the rats were anesthetised with 4% isofluorane (Merial Animal Health Ltd, UK) during induction, then ~3% isofluorane for maintenance of the anesthetic plane. 100% oxygen was

provided for the duration of the surgery. The rats head was shaved with the aid of fur clippers and the rat was then fixed into a stereotactic frame with the use of ear bars to ensure the skull remained stationary during the entirety of the procedure.

The skull was exposed by cutting and retracting the scalp, after numbing the area with lidocaine (5% Lidocaine ointment, Teva UK Ltd., UK). Using a Kopf scaled probe, flat skull measurements were taken at both lamda and bregma points to ensure that the two dorso-ventral measurements were within 0.5mm of each other before surgery could proceed. To provide access to the brain, a small piece of skull was removed, above the injection sites. The lesion surgery consisted of 4 separate injections of 0.09M NMDA in phosphate buffer (PB) solution into the following locations, relative to bregma; Injection point 1: AP -1.7, ML +0.2, Injection point 2: AP -2.4, ML +0.2, Injection point 3: AP -2.4, ML -0.2, Injection point 4: AP -1.7, ML -0.2 with a DV of -7.4 for all 4 injection points. The NMDA solution was injected into the target area with a 1.0µl Hamilton syringe and a MicroSyringe Pump Controller (Micro 4; World Precision Instruments Inc) at a rate of 25nl per minute for 4 minutes, totalling in 0.1µl total injection volume per injection site. Correct flow was determined between each injection to ensure no blockages within the needle had occurred. After each injection had taken place, the needle was maintained in the same position for a further 4 minutes to ensure the NMDA solution had properly dispersed. For the sham surgeries, the needle was inserted into the 4 injection sites sequentially and was left in each position for 1 minute without injection of any liquid.

Following intracerebral injection, the incision site was first cleaned and then sutured using 4-0 gauge Mersilk suture kit (Ethicon, USA) and veterinary wound powder (2% w/w tosylchloramide sodium; Battles, UK) was applied. Hypromellose (0.3% w/v) containing eye drops (Blumont, USA) were used throughout the surgery to prevent the eyes from drying out. Subcutaneous injections of glucose saline (0.9% w/v sodium chloride and 5.0% w/v glucose; Aquapharm No3, Animalcare Ltd., UK) were given twice during the surgery, at 2.5ml each to spread out the volume received. Intramuscular injection of 0.1ml clamoxyl was given as a prophylactic antibiotic, along with 0.05ml Vetgesic (0.3mg/ml buprenorphine; Sogeval UK Ltd., UK) for pain management. Throughout the surgery, the rat's normal body temperature was maintained with the use of a heated mat. The hind claws were trimmed with cutters and the rat was placed into a heated recovery box until it was able to self-right itself. Following this, the rats were returned to a cage lined with cardboard for 24hr with food and water available *ad libitum*. Weights were checked and compared to the pre-surgery weight daily for 5 days post-surgery to ensure the rat started gaining weight.

2.3. Bow-tie maze task

The bow-tie maze task (based on Albasser *et al*., 2010) consisted of a pretraining phase, taking 6 days, and a training phase, also taking 6 days, followed by a final test day. The NRe-lesioned and sham lesioned rats from each cohort were subdivided into two groups each: Lesion-Novel, Lesion-Familiar, Sham-Novel and Sham-Familiar. While all four groups underwent the same pretraining, training and test procedure, the protocols for Lesion-Novel/Sham-Novel and Lesion-Familiar/Sham-Familiar differed in the object sets the rats were exposed to during the training phase.

2.3.1. Handling

Following surgery and a recuperation time of 2 weeks, the rats were subsequently handled on a daily basis prior to pretraining. The handling allowed the rats to become accustomed to being picked up, held and transferred from place to place.

2.3.2. The bow-tie maze apparatus

The behavioural task took place in a maze (Figure 2.1) constructed out of folded 1.5mm shee*t al*uminium with a 18mm thick plywood base. The maze consisted of two triangular shaped arenas joined together via a central corridor at the apex of each triangle. The dimensions of the maze are as follows; 1.2m in length, 0.5m width, 0.5m height with the central corridor being 0.12m wide, 0.2m long. A central non-transparent vertical free sliding door separates the two arenas. Objects were placed into the two corners at the ends of the maze. One food well was attached centrally to the floor at each end of the maze and therefore ensured that any food reward placed into it was not associated with either of the presented objects.

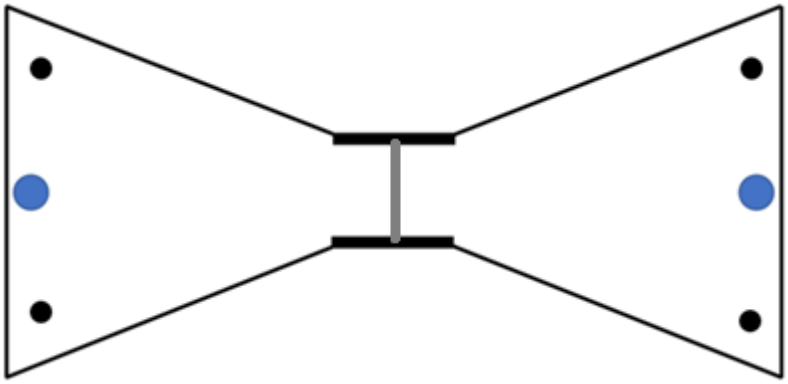

Figure 2.1: Plan view diagram of the bow-tie maze. The food wells are represented by blue circles. The approximate location of the object placement is represented by the black circles. The movement of the rat in the maze could be controlled by a vertical sliding door in the centre of the maze.

2.3.3. Object procurement

Specific criteria were used for procurement of the experimental objects. The objects chosen to be used in the experiment consisted of a range of ‘everyday’ household items, toys and other junk objects (see Figure 2.2 for an example object set). The objects were chosen based on size, shape, tactility, appearance and material, with exclusion criteria covering any objects that exhibited strong smells, moving / heavily protruding parts or were liable to fall over during the experiment. Efforts were made to ensure objects presented together were of similar complexity and size to prevent bias based on a differential level of interest. Between pretraining or training sessions the objects were cleaned with 100% ethanol to eliminate olfactory cues.

Figure 2.2: Example set of objects used in a single session.

2.3.4. Pretraining

Rats underwent daily pretraining for 6 days, in order to learn to shuttle from one end of the maze to the other and collect a food reward, when the central door was opened. The central door was only in place for days 4-6 of the pretraining protocol. On day 1, sucrose pellets (20mg blue sucrose pellets) were scattered around the maze, including the food wells. The rats were placed into the maze in pairs and were allowed to explore freely for 20 minutes. On days 2 and 3, the rats were placed into the maze one at a time for 20 minutes. Sucrose pellets were placed only in the food wells and these were constantly rebaited, to promote shuttling from one end of the maze to the other. This process was repeated on days 4 and 5, with the difference that the central door was used to control the movement of the rats. On day 6, rats were again encouraged to shuttle from end to end in the maze whenever the central door was opened. In

addition, three different object pairs were placed in the maze, to allow the rat to habituate to the presence of objects. Pretraining objects were not part of the object sets used in the training phase of the task.

2.3.5. Training

In the training phase, the rats were individually subjected to two sessions per day over a 6 day period (sessions 1-12). One session took place in the morning and one in the afternoon. Each training session followed the same protocol and consisted of one ‘pre-trial’ followed by 20 consecutive trials of 1 minute each. At the start of the session the rat was placed into one side of the maze with no objects and the central door closed to habituate to the environment. At the start of each trial the central door was raised to encourage the rat to shuttle to the other end of the maze, where it was allowed to collect 2-3 sucrose pellets from the food well and explore two objects for a total of 1 minute, before the central door was raised again. After the final trial, the central door was opened and the rat moved to the other end of the maze that was now empty, before being lifted out of the maze. In the ‘pre-trial’ the object pair consisted of one pre-training object and one object of the training set. In each consecutive trial, the object pairs consisted of one object that the rat encountered for the first time in this training session and an identical copy of the object it had just seen in the preceding trial. The position of each object upon the second encounter, in relation to its previously viewed copy (same side, opposite side) was counterbalanced across each session. During all training sessions along with the final test session, the exploration behaviour of the rats was captured by video recording, to later be played back offline, in order to score the footage for later analysis.

A total of 147 unique objects were used in duplicate for the entire training phase. One set of 21 objects (plus their respective identical copies) was designated the ‘familiar’ object set. Groups Sham-Familiar and Lesion-Familiar saw the same ‘familiar’ object set in each of the 12 training sessions, to enable the rats to become highly familiarised to these objects over the course of the training. The order of the objects, and therefore the object pairings, differed between each session. The remaining objects were separated into 6 sets of 21 duplicate objects each. Sham-Novel and Lesion-Novel rats were exposed to these ‘novel’ object sets over the first 6 training sessions. In the last 6 training sessions, the rats explored the same 6 ‘novel’ object sets, however the order of the objects within each set was altered.

2.3.6. Test day and perfusions

The test day occurred with a single session (session 13) whereby the entire cohort of rats were subjected to the 'familiar' object set used for the previous 12 training sessions for the Sham-Familiar and Lesion-Familiar groups. The order of the objects was again changed. At the end of each session the rat was then placed back into its original cage and left in a darkened room for 80 minutes. The rat was then given an intra-peritoneal injection of 1ml Euthatal (sodium pentobarbital; Rhône Mérieux, UK) to induce a deep anesthetised state over a period of approximately 10 minutes. Ninety minutes following the end of the behavioural experiment, the rat was then transcardially perfused with a solution of 0.1M phosphate buffer (pH 7.4, 300ml), followed by 0.1M phosphate buffer (PB) with 4% paraformaldehyde (pH 7.4, 300ml). Following this the brain was extracted and suspended in 0.1M PB with 4% paraformaldehyde for 2 hours, then transferred to a 30% sucrose solution for 2 days at 4°C. Due to the time constraints of the test day protocol, the perfusions were performed by Dr Clair Booth.

2.3.7. Statistical analysis

Exploratory behaviour of the rats in sessions 1 and 13 was scored manually using a custom-made scoring software developed by Dr Silviu Rusu. Behavioural scoring of the rat occurred when the rat's nose was directed towards the object and within a distance of 1cm from the object, classed as object exploration. Sitting on the object or looking up while resting against the object, along with biting of the object, was not counted as exploratory behaviour. The total cumulative exploratory behaviour over all 20 trials of each session was calculated. Furthermore, the discrimination ratio d2 was calculated as a measure of performance in the task, which takes into account subtle differences in the total levels of exploration between rats. For Sham-Novel and Lesion-Novel groups, d2 was calculated as the relative difference in exploration time (E) between the novel object and the familiar object (just seen on the previous trial), divided by the total exploration time in the trial:

$$d2\ (Group\ Novel) = \frac{E_{novel} - E_{familiar}}{E_{total}}$$

This definition of d2 was also correct for Sham-Familiar and Lesion-Familiar groups in session 1 only, when the rats were exploring the 'familiar' object set for the first time. For sessions 2-13 of groups Sham-Familiar and Lesion-Familiar, the discrimination ratio d2 was calculated as the

relative difference in exploration time between the less recently seen familiar object (last explored in the previous session) and the more recently seen familiar object (last explored on the previous trial), divided by the total exploration time:

$$d2\ (Group\ Familiar) = \frac{E_{less\ recent} - E_{more\ recent}}{E_{total}}$$

The discrimination ratio was recalculated after every trial of a session, based on the cumulative exploration over the preceding trials, to yield the updated discrimination ratio. Repeated measures ANOVA was used to determine main effects of surgical procedure (sham/lesion), stimulus type (novel/familiar) and session (first/final), along with interaction effects. The one sample t-test was used to assess if the mean updated discrimination ratio for each group was significantly different from zero, i.e. if the rats showed significant discrimination. Statistical analysis was performed using SPSS statistics 23 (IBM Corp., USA).

2.4. Analysis of brain sections

2.4.1. Tissue preparation

The brains were prepared for slicing one at a time. A brain was removed from the 30% sucrose solution and lightly patted dry. About 80% of the cerebellum was removed across the coronal plane of the brain with a scalpel blade and the brain was placed on a circular mounting block that had been covered in a layer of cryomatrix (Thermo Scientific, USA). The cryomatrix was ensured to have surrounded the remaining cerebellum as to provide a substantial fixture to the mounting block after freezing. The brain and the cryomatrix were frozen in isopentane, chilled using liquid nitrogen. The assembly was then transferred into the cryostat (CM3050 S, Leica UK) and was allowed to equilibrate for 30 minutes. Coronal sections of 40µm thickness were cut at -22°C. Sections located around the NRe lesion site were collected directly onto microscope slides for cresyl staining to confirm the correct location and extent of the lesion (see section 2.4.2.). The remaining brain slices were collected into netted wells with PBS for subsequent c-fos analysis using immunohistochemistry (see section 2.4.3.) or placed into cryopreservant solution (0.1M Sodium Phosphate monobasic (pH 7.4), 20% Glycerol, 2% Dimethyl Sulfoxide (DMSO)) for long-term storage at -20°C.

2.4.2. Cresyl staining

Microscope slides were dehydrated and incubated with cresyl stain (1g cresyl violet in 1L ddH_2O, 2.5ml glacial acetic acid) as described in Appendix, Table A.1 The slides were cover-slipped with DPX Mounting Medium (Raymond A Lamb, UK) and 0.13 - 0.17 mm thick glass coverslips, with sufficient pressure applied to remove superfluous DPX mounting media from between the slide and coverslip. The slides were then left to dry for a further 72 hours before any cured DPX was scraped off and the slide cleaned with lint free microscope paper tissues and absolute ethanol.

2.4.3. Immunohistochemistry

Immuno, ABC and DAB staining

Brain slices were washed in peroxidase block solution (1% H_2O_2 in PBS) for 10 min. After 4 washes in PBST (0.1M PBS with 0.2% Triton X-100), the slices were blocked in 5% S-1000 normal goat serum (Vector Laboratories, UK) and 2.5% bovine serum albumin (BSA) in PBST for 1hr at room temperature. The blocking solution was then removed and rabbit polyclonal primary anti c-fos antibody (abe457; Merck Millipore Corp, USA) was added at a dilution of 1:20,000 (diluted in in blocking solution). Following 24hr incubation at 4°C, the netted wells containing the brain slices were agitated on a shaker for 2h, before being incubated for a further 22hr at 4°C, totalling an incubation of 48hr. Four washes in PBST were followed by a 2hr incubation at room temperature with biotinylated goat anti-rabbit secondary antibody (BA-1000; Vector Laboratories, UK) at a dilution of 1:200 in blocking solution. To visualise the bound biotinylated secondary antibody, brain slices were first incubated with the avidin-biotinylated horseradish peroxidase complex (ABC) reagent (Vectastain Elite kit; Vector Laboratories, UK) according to manufacturer's instructions. After 6 washes in PBST and 2 washes in 0.05M Tris buffer, addition of the diaminobenzidine (DAB) substrate (Vector Laboratories, UK), which is converted by the horseradish peroxidase complex, led to the production of a dark brown reaction product, which is visible to the naked eye. Once the desired colour was achieved, cold PB (0.1M pH 7.4) washes were used to stem the staining reaction further.

Mounting and drying

Following the immunohistochemical stage, the brain slices were subjected to three wash steps in cold PB, before being refrigerated overnight at 4°C. The slices were then transferred to a glass dish containing PB with 10% ethanol to aid mounting onto the glass Polysine microscope slides (Thermo Scientific, UK). The slices were left to dry for a period of 72 hours to ensure the

complete evaporation of water in the interface layer between the brain slice and microscope slide.

Dehydrating and cover-slipping

The microscope slides were subjected to a series of wash baths with increasing concentrations of ethanol from 50% to absolute ethanol, to further dehydrate the brain slices in preparation for cover-slipping. After the dehydration washes, the slides were then transferred to a series of Xylene wash baths until being cover-slipped as described above (see section 2.4.2.).

2.4.4. Microscope analysis of c-fos positive nuclei

Brightfield images of the sections were initially taken at 1.25x magnification with a Leica DM6B upright light microscope and connected digital camera (Orca-flash 4.0; Hamamatsu Photonics, Japan) in order to select the sections to be used for the analysis. The sections were also screened for suitability; the condition of the brain tissue and slices with substantial damage, distortion and heavily overlapping areas were subsequently discarded from further analysis.

Consecutive tilescans of viable sections were then taken at 10x magnification to be later stitched together to form a merged composite image of the entire brain section. The stitching process was achieved through the use of a self-developed macro created within Fiji (ImageJ) to ensure accurate alignment of the tilescans to form a merged composite image. The process also ensured the minimisation of distortion during the stitching process. This approach was deemed advantageous through the subsequent saving of each brain section with the corresponding set of ROIs overlaid on top for future reference.

Regions of interest (ROI) with length of 0.94mm and width 0.67mm were taken from various subfields of the hippocampus, medial prefrontal cortex, perirhinal cortex and neighbouring regions (Table 2.1), brain regions considered part of the recognition memory network. ROIs in the visual cortex and motor cortex were taken as control regions, which were not expected to show differential c-fos expression in response to novel and familiar objects.

Table 2.1: List of brain regions. Brain regions that were analysed for levels of Fos-positive nuclei area given with their corresponding locations relative to bregma.

Area of brain	Location relative to Bregma (mm)
CA1 – dorsal (DCA1)	-2.52
CA1 – intermediate and ventral (iCA1, vCA1)	-4.80
CA3 – dorsal (DCA3)	-2.52
CA3 – intermediate and ventral (iCA3, VCA3)	-4.80
Dentate gyrus – dorsal (DDG)	-2.52
Dentate gyrus – intermediate and ventral (IDG, VDG)	-4.80
Perirhinal cortex (PRH)	-5.3 to -6.3
Prelimbic cortex (PRL)	4.2 and 2.7
Infralimbic cortex (IFC)	2.7
Anterior cingulate cortex (ACC)	4.2
Medial orbital cortex (MOC)	4.2
Ventral orbital cortex (VOC)	4.2
Dorsal peduncular cortex (DPC)	2.7
Subiculum – dorsal and ventral dSUB, vSUB)	-5.16
Temporal association cortex (TE2)	-5.3 and -6.3
Entorhinal cortex (ENT)	-7.3 and -8.3
Postrhinal cortex (PSTC)	-7.3 and -8.3
Motor cortex M2 (M2)	4.2 and 2.7
Visual cortex V2 (V2)	-4.80

ROIs were taken using Fiji and were processed with the aid of a macro which rotated all the ROIs to the horizontal plane, renaming them as sub images of the original image. The macro also saved a ROI overlay image for future reference. For each brain section, a coma separated variable file was created with the number of each ROI and its corresponding bregma position and brain region. Schematics of ROIs taken are given in Appendix (Figures A.1-4) and an example of subfields of the medial prefrontal cortex at 2.70mm from bregma is provided in Figure 2.3).

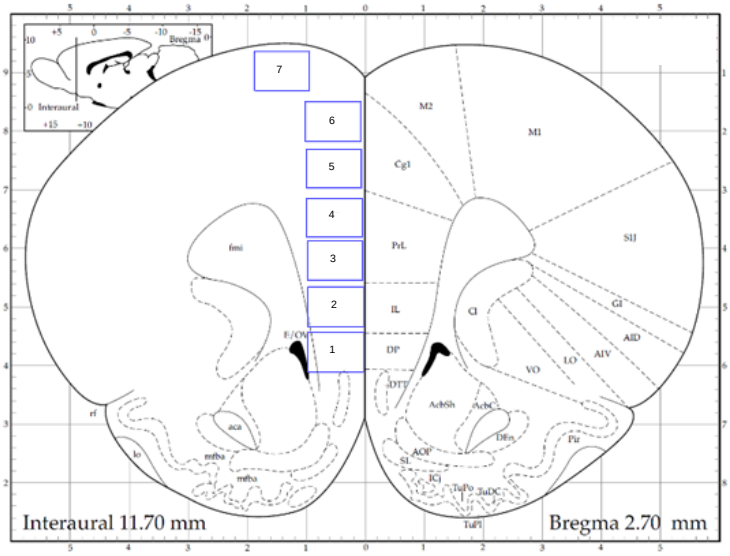

Figure 2.3: Example image of brain section with accompanying regions of interest. Regions of interest that were taken from both hemispheres for dorsal peduncular cortex (DP), infralimbic cortex (IL), prelimbic cortex (PrL), anterior cingulate cortex (Cg1) and motor cortex (M2) are indicated by numbered rectangles outlined in blue. Figure adapted from Swanson atlas, 1998.

2.4.5. ROI Pipeline – modular image analysis for c-fos cell counting

Previously used methods for the accurate classification and counting of Fos positively stained nuclei were met with various limitations, which the current approach served to mitigate. Approximately 6000 ROI images required analysis so in close collaboration with Dr S. Cross from the Wolfson Group, University of Bristol, a superior method for cell detection and counting was developed for the batch-processing required for analysis.

The process involved the use of the Modular Image Analysis (MIA) plugin, a plugin that had been previously produced and continuously updated within the Wolfson Group, capable of providing a modular framework for assembling image and object analysis pipelines. In this case, the MIA plugin was configured to incorporate the use of the Waikato Environment for Knowledge Analysis (Weka) GNU plugin, originally developed at the University of Waikato, New Zealand to be trained to distinguish and quantify the DAB stained cells within each brain section of the experiment.

The Weka plugin uses a machine learning component that was utilised in this case for cell detection. The plugin incorporates a training stage, in which a classifier model is created, based on a selection of randomly chosen ROI images taken from each cohort to provide a representative approximation of all images to be analysed. Multiple areas within each image were manually designated one of three components: ‘cell’, ‘tissue’ or ‘tear/void’ by marking the areas as one of the three objects. The model was then trained and was subsequently used within the MIA pipeline to detect the various components within the ROI image, counting the number of cells that satisfied the criteria the model had been trained upon (Figure 2.4).

Through the use of the Weka plugin, the MIA pipeline loaded an image, detected the areas of the image that corresponded to stained nuclei, accepting only the round or oval shaped cells that fit within specific criteria, including a cell circularity of 0.75, 2-78µm in diameter and a maximum axial ratio of 2.7. Areas of the image containing voids or tears over 130µm^2 in size were classified as such. By default, the area of each classified tear/void was automatically increased by 5% to account for the typically darker edges. These areas were included as area measurements within the exported data, to be factored into the cell density calculations. Tears and voids were subsequently discarded from analysis. The quantified data including the cell count was exported to an excel spreadsheet for later analysis.

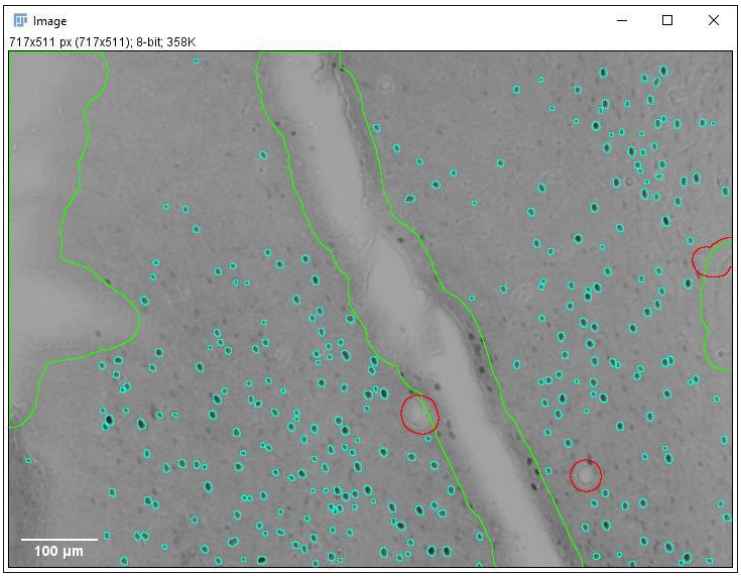

Figure 2.4: Representative example of modular image analysis output. The MIA pipeline was trained to detect Fos-positive nuclei (teal), along with voids (green) and tears (red) in the region of interest. This example ROI image was taken from the prelimbic region of the mPFC, within the coronal plane, at Bregma 2.70.

For each ROI, the mean Fos count per mm^2 was calculated for each rat. Differences in the levels of Fos-positive nuclei were analysed using Two-Way ANOVA to test for main effects of surgical procedure (sham/lesion) and stimulus type (novel/familiar), along with interaction effects.

2.4.6. Cresyl analysis

Full coronal images were created by taking consecutive tiled images (tilescans) of the cresyl sections using an automated XY microscope stage, to then be automatically stitched together using Leica Application Suite (LAS) X software (build 3.3.3.1). The resulting merged images were subsequently saved as LIF project files, exported to TIF images for analysis. The tile scanned images were taken at 10x magnification using a Leica DMI 6000B microscope with a Leica CTR6500 lightbox and Leica DFC365 FX camera module according to the following coordinates provided in Table 2.2.

Table 2.2: Brain sections taken for cresyl analysis. Positions of selected brain sections relative to bregma, along the anterior-posterior axis.

Position relative to Bregma	Swanson (1998) Atlas equivalent level
-1.53	level 25
-2.00	level 27
-2.45	level 28
-2.85	level 29
-3.25	level 30

A semi-automated method for analysing the extent of the lesion within the rat brains had been developed (again in close collaboration with Dr S. Cross from the Wolfson Group, University of Bristol) with the use of the MIA plugin, re-configured for this purpose. The pipeline was set to run in a semi-batch mode configuration, one Bregma level at a time (levels 25, 27-30). For each Bregma level, a brain overlay taken from the Swanson atlas (Swanson, 1998) in the form of a scalable vector graphic. Thalamic nuclei regions were subsequently added as solid colour filled objects within each overlay. Each thalamic region consisted of its own unique ID for later identification. The image in Figure 2.5 below demonstrates the overlay used for level 25 of the Swanson atlas. The overlay images were then exported as tif images and were used individually in the analysis process.

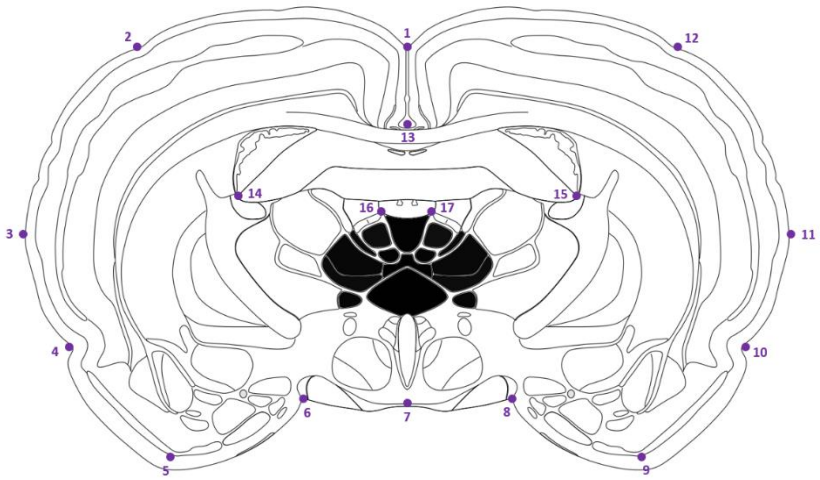

Figure 2.5: Overlay used for lesion analysis. An example overlay used for lesion analysis of cresyl-stained level 25 sections. Thalamic brain regions analysed are shown in black. The pre-drawn consecutive points are shown in small purple points with adjacent labelled numbers. Overlay taken from Swanson, 1998.

For each set of images to be analysed, the corresponding reference brain overlay was first loaded into the MIA pipeline along with a folder containing all the cresyl stained brain sections corresponding to that level (for example, level 25). The reference brain overlay (see Figure 2.5) had pre-drawn consecutive points manually placed on the overlay. These points were matched to equivalent points, again manually drawn on each of the brain sections to be used to locate and superimpose the brain overlay, over the brain section, matching as closely as possible, the various brain regions making up the brain section. The pipeline then served to compartmentalise each thalamic nucleus, based on the superimposed overlay, quantifying and exporting to an excel spreadsheet, the projected area of each nuclei, along with the potential lesioned area within it. For each thalamic nucleus, the sum of the area was summed across the 5 levels to compute the total area per nucleus. Subsequently, for each rat in groups Lesion-Novel and Lesion-Familiar, the lesion size (% lesion) relative to the mean nuclei area in the sham groups was calculated.

2.5. Bayesian modelling using RStan

The Stan software (Carpenter *et al*., 2017) was used for the Bayesian modelling analysis through the use of the RStan package (R package version 2.17.3, 2018) within R (version 3.4.3, 2017).

A hierarchical model (Figure 2.6) was established that included partial pooling of cell count means across experimental groups, and then across brain regions. The model assumes that the experimental Fos counts $y_{i,j,k}$ (i being the index for each individual rat; j, the brain region index for each of n_r = 23 brain regions; k, the index for each of n_g = 4 experimental groups) are independent of each other but are sampled from a normal distribution N defined by a mean $\theta_{j,k}$ and a standard deviation $\sigma_{j,k}$:

$$y_{i,j,k} \sim N(\theta_{j,k}, \sigma_{j,k})$$

Equation 2.1

The partial pooling approach assumes that the means $\theta_{j,k}$ are sampled from a set of normal distributions, one for each brain region, defined by a per-region mean μ_j and a standard deviation τ_j:

$$\theta_{j,k} \sim N(\mu_j, \tau_j)$$

Equation 2.2

Lastly, the brain region means are modelled as being sampled from one global normal distribution:

$$\mu_j \sim N(\mu_{global}, \tau_{global})$$

Equation 2.3

Equations 2.1-2.3 can be described as the likelihood functions of the Bayesian model. Prior distributions were specified for $\theta_{j,k}$, μ_j and μ_{global} and their associated standard deviations. For each mean, priors were normal distributions, for the standard deviations they were Cauchy distributions centred on zero and restricted to be non-negative. For μ_{global} the mean of the prior normal distribution was centred on the frequentist mean over all the experimental Fos counts.

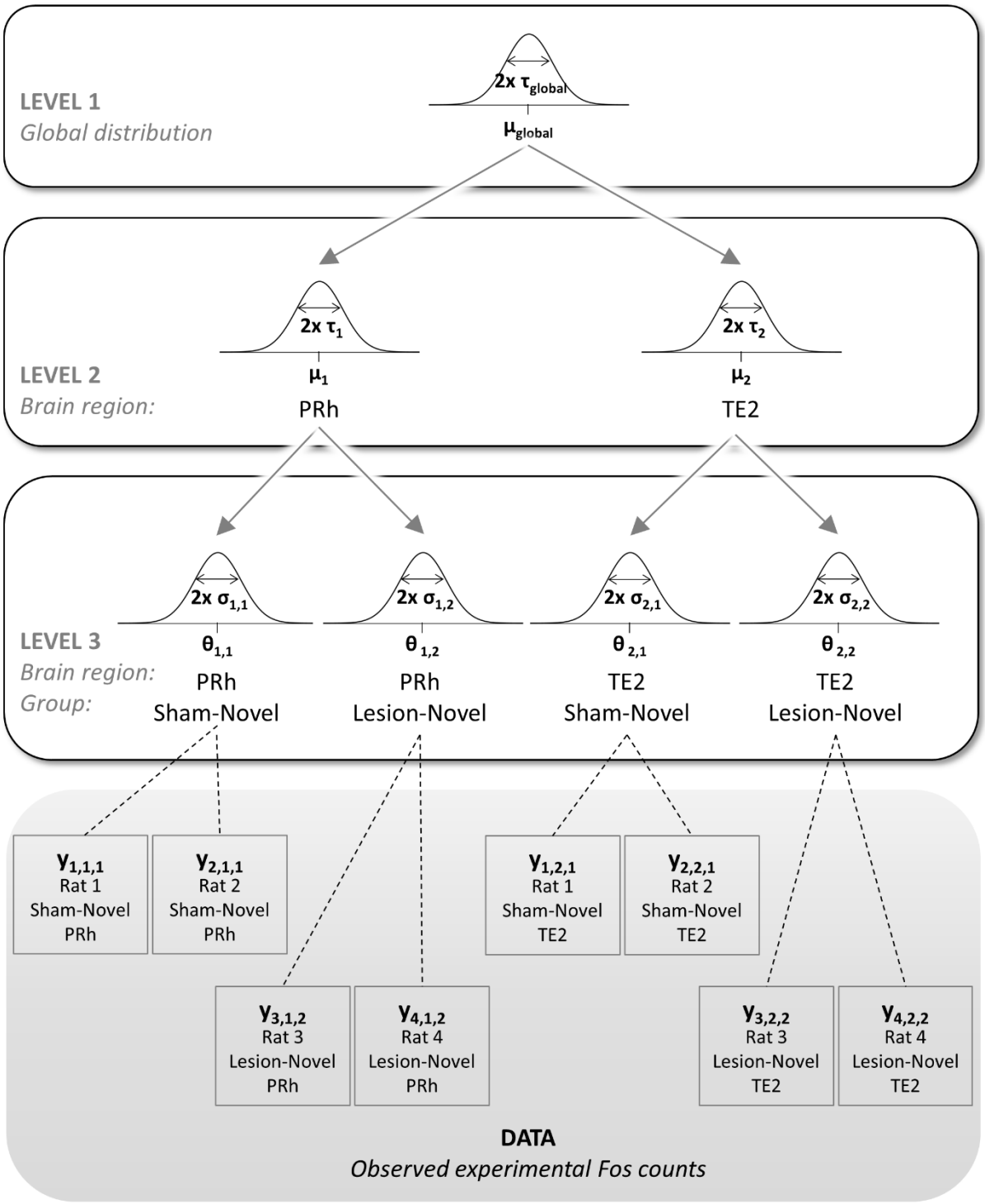

Figure 2.6: Bayesian hierarchical model. A diagram of the Bayesian hierarchical model implemented in the analysis is shown for a subset of rats (1-4), brain regions (PRh,1; TE2, 2) and experimental groups (Sham-Novel, 1; Lesion-Novel, 2). Estimated parameters on each level of the hierarchy are described by normal distributions with a mean ($\theta_{j,k}$, μ_j, μ_{global}) and a standard deviation ($\sigma_{j,k}$, τ_j, τ_{global}), with j referring to the brain region index and k to the experimental group index.

As it is impossible to solve this hierarchical model analytically, as it includes multiple unknown parameters, RStan uses Hamiltonian Monte Carlo simulations to generate samples from the posterior probability distribution, which can then be used to estimate the model parameters (Figure 2.7). RStan ran four Markov chains simultaneously on separate computer cores to increase the number of posterior samples obtained in a shorter period of time and to confirm consistency of sampling across the chains. A total of 2000 iterations were completed per chain, which included 1000 warm-up iterations and 1000 sampling iterations. Only the latter were included in the analysis.

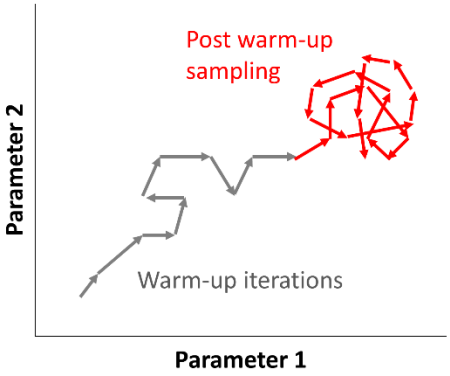

Figure 2.7: Graphical representation of a Markov chain exploring 2-dimensional parameter space. The Markov chain starts sampling randomly in parameter space. Using Hamiltonian Monte Carlo method, the chain explores parameter space, making its way towards a region where the samples more closely match the data, with higher probability and lower error. For the model in the present study, the number of parameters to be estimated were 92, therefore the simulation took place in 92-dimensional parameter space.

2.6. Analysis of RStan fit

Theta samples generated by the fit, along with their respective mean values, were extracted from the RStan fit object. The correlation between estimated mean thetas and their respective frequentist sample means was calculated by linear regression analysis. To determine the difference between the spread of the Bayesian means and the spread of the frequentist means, a one-sample t-test was used to compare the slope of the linear regression to a slope of 1. All graphs were produced using the ggplot2 package in R (Wickham, 2016).

2.6.1. Pair-wise comparisons of estimated thetas

For each brain region, estimated theta values were compared pair-wise between the four experimental groups, by using Null Hypothesis Significance Testing (NHST) and by calculating the probabilities of one theta being larger than the other.

Null Hypothesis Significance Testing

NHST is a standard test in frequentist statistics. Here it was used to compare two sets of theta samples that had been estimated using the Bayesian modelling. For each theta pair, one was designated θ_A and the other θ_B. The difference between the mean of all θ_A samples and the mean of all θ_B samples was calculated ($\Delta\mu$). The null hypothesis was that θ_A and θ_B are not different from each other. Under the null hypothesis both θ_A and θ_B sample sets were drawn from the same distribution and the observed difference between them ($\Delta\mu$) occurred purely by chance. The alternative hypothesis was that θ_A and θ_B sample sets were indeed different from each other. A diagram of the NHST approach is shown in Figure 2.8.

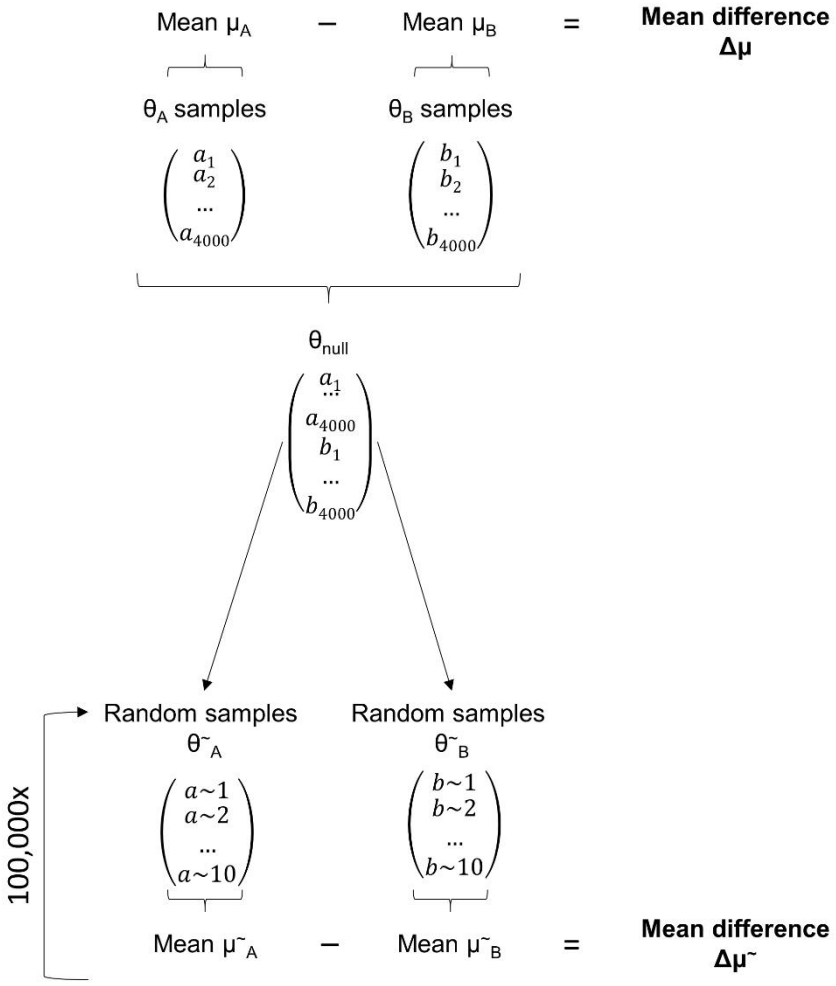

Figure 2.8: Null Hypothesis Significance Testing. The two sets of theta samples that are to be compared by Null Hypothesis testing (θ_A and θ_B) are combined and random samples are drawn from this joint sample set θ_{null} to produce two random sample sets ($\bar{\theta}_A$ and $\bar{\theta}_B$). The means of the two random sample sets are calculated and the differences between the means is determined ($\Delta\bar{\mu}$). In total, 100,000 iterations of the sampling step are performed. The mean difference between the actual sample sets ($\Delta\mu$) can then be compared statistically with the density distribution of the computed $\Delta\bar{\mu}$ values.

To perform the NHST, all θ_A samples were combined with all θ_B samples to create a combined sample set, termed θ_{null}. From θ_{null} 10 random samples (equivalent to the number of replicates in the actual experiment) were drawn with replacement. This new sample set was termed $\tilde{\theta}_A$. The step was repeated to create a $\tilde{\theta}_B$ sample set. The difference between the mean of $\tilde{\theta}_A$ ($\tilde{\mu}_A$) and the mean of $\tilde{\theta}_B$ ($\tilde{\mu}_B$) was calculated (termed $\Delta\tilde{\mu}$). This sampling set was then repeated 100,000 times. The resulting 100,000 $\Delta\tilde{\mu}$ values can be plotted as a histogram with an approximate Gaussian distribution centred close to zero (Figure 2.9). To obtain the *p* value, the proportion of $\Delta\tilde{\mu}$ values that were greater than $|\Delta\mu|$ was added to the proportion of $\Delta\tilde{\mu}$ values that were smaller than $-|\Delta\mu|$. The resulting *p* value represents the probability that the observed difference in the data ($\Delta\mu$) occurred by chance if the null hypothesis (that there is actually no difference between θ_A and θ_B) was true. If $p < 0.05$ the null hypothesis was rejected.

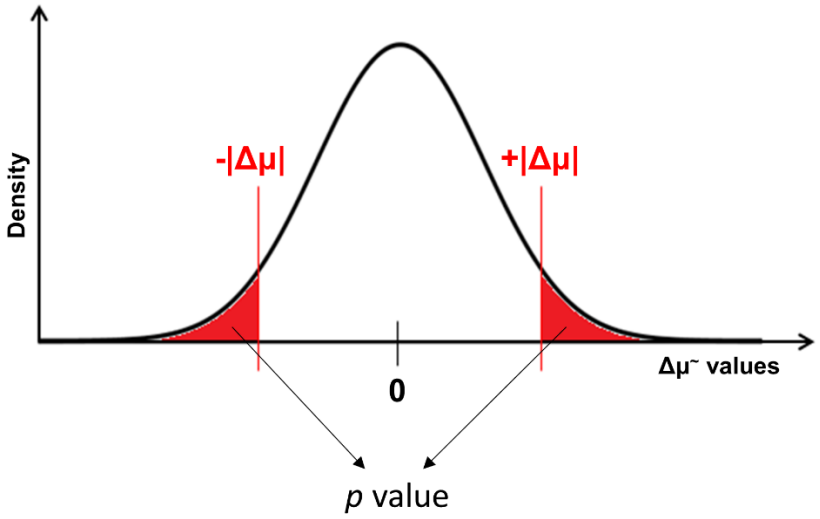

Figure 2.9: Distribution of $\Delta\tilde{\mu}$ values. The distribution of $\Delta\tilde{\mu}$ values calculated as part of Null Hypothesis Significance Testing can be described as a density plot, centred around zero. The p value of the significance test is calculated as the sum of the proportion of $\Delta\tilde{\mu}$ samples larger than the absolute value of $\Delta\mu$ (the mean difference between the two theta sample sets that are being compared) and the proportion of $\Delta\tilde{\mu}$ samples that are smaller than the negative of the absolute values of $\Delta\mu$.

Calculation of probabilities

A different approach to investigate the difference between two theta sample sets is to calculate the probability that one theta (e.g. θ_A) is larger than another (e.g. θ_B). To achieve this, the proportion of samples in θ_A that are larger than their counterparts in the θ_B sample set is calculated. If this resulting probability is close to 1, it is likely that θ_A is larger than θ_B, whereas if

it is close 0, it is highly likely that θ_A is smaller than θ_B. Probability values close to 0.5 indicate that there is no difference between θ_A and θ_B.

2.6.2. Comparison between Bayesian and frequentist approaches

While the precision of the Bayesian and frequentist approaches can be examined by comparing the uncertainties associated with the estimated theta values (Bayesian) and the calculated sample means (frequentist), comparing the accuracy of the Bayesian and frequentist approaches is difficult, as the true mean of the population is unknown. To remedy this, simulated data sets were generated based on the posterior predictive distributions from the RStan fit, defined by each mean theta and associated sigma. For these simulated data sets the true mean is known, as it is the mean theta values. By running frequentist statistics and Bayesian analysis on this simulated data set, it is possible to ascertain the difference of the resulting sample means and new estimated theta values from the true mean and establish the accuracy of the two statistical approaches.

A set of 10 simulated samples (equivalent to n=10 in the actual experiment) were drawn from the posterior predictive distribution for each estimated theta (now termed the 'true mean'). For the frequentist analysis, the sample mean of each simulated data set was calculated. The differences between the sample means and their respective true means were determined by computing the sum squared error, i.e. the sum of the squared difference between each sample mean and the true mean. For the Bayesian statistics the simulated sample sets were processed using RStan, as described above (see section 2.5.). The resulting mean theta values were compared to their respective true means, by calculating the sum squared error as described for the frequentist analysis. Following 10 iterations of the above-mentioned steps, the mean of the 10 sum squared errors were taken for both the frequentist and the Bayesian approaches and plotted on a graph for comparison.

3. Results

3.1. Lesion analysis

Substantial cell loss in the NRe was observed across NRe-lesioned animals (Figure 3.1). Along the anterior-posterior axis, the greatest cell loss was in most cases observed in the anterior regions. At -1.53 mm relative to bregma the extent of the lesion in the NRe was 25.3% +/- 6.02% (mean +/- s.e.m.; max 97.2%, min 0%). In those rats in which no tissue loss was detected in the anterior sections, lesioning of the NRe was detected at the more posterior levels; at -3.85 mm relative to bregma the mean NRe lesion area was 17.3% +/- 3.88% (max 47.1%, min 0%). Some lesioning of the NRh was observed in most lesioned rats. The greatest extent of NRh cell loss was observed at -2.00 mm relative to bregma (15.9% +/- 5.13%; max 65.5%, min 0%), while in all other sections the tissue loss was < 10% of the structure. In several rats, additional damage occurred within interanteromedial nucleus thalamus (18.9% +/- 7.95%), paraventricular nucleus thalamus (16.2% +/- 11.5%) and paratenial thalamic nucleus (16.6% +/- 8.23%). In all other thalamic nuclei, cell loss was <10% of the structure.

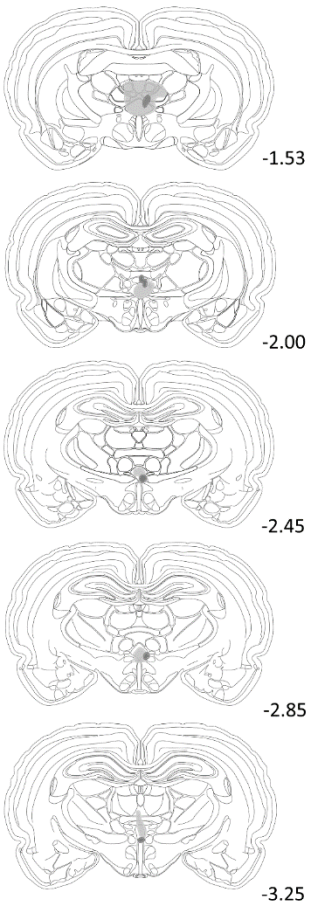

Figure 3.1: Largest and smallest NRe lesions. Diagrammatic reconstructions of the largest NRe lesions (light grey) and the smallest NRe lesions >5% (dark grey).

3.2. Behavioural data

In the first session of the bow tie maze task, all rats were able to discriminate between the object they had just encountered in the previous trial, and an entirely new object (Figure 3.2). In contrast, in the test session all groups showed reduced discrimination compared to the first session and both groups that explored highly familiar objects (groups “Sham-Familiar” and “Lesion-Familiar”) were unable to discriminate between the objects shown (Figure 3.2). Repeated-measures ANOVA revealed a significant main effect of type of session (first session vs last session; $F(1, 36) = 28.271$, $p < 0.001$) and a significant main effect of type of stimulus (novel vs familiar; $F(1, 36) = 12.724$, $p = 0.001$). In the first session, all four groups discriminated significantly, as determined by one-sample t tests (difference from a discrimination ratio of zero; Sham-Novel: $t(9) = 8.845$, $p < 0.001$; Sham-Familiar: $t(9) = 8.533$, $p < 0.001$); Lesion-Novel: $t(9) = 8.010$, $p < 0.001$; Lesion-Familiar: $t(9) = 9.686$, $p < 0.001$). Sham-Novel and Lesion-Novel rats also showed significant discrimination in the test session (Sham-Novel: $t(9) = 3.148$, $p = 0.012$; Lesion-Novel: $t(9) = 4.505$, $p = 0.001$), while Sham-Familiar and Lesion-Familiar rats showed discrimination that was not significantly different from zero (equal discrimination of novel and familiar object; Sham-Familiar: $t(9) = 0.495$, $p = 0.632$; Lesion-Familiar: $t(9) = 1.545$, $p = 0.157$).

In summary, while the Sham-Novel and Lesion-Novel groups were able to discriminate in the first session and the test session, Sham-Familiar and Lesion-Familiar were unable to discriminate between highly familiar objects in the test session. Furthermore, no differences between sham and NRe-lesioned rats were observed.

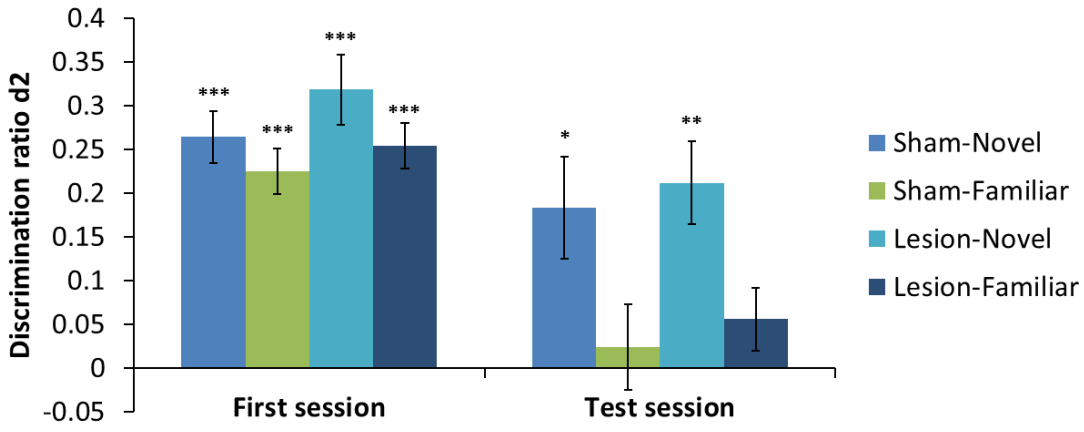

Figure 3.2: Discrimination ratio in the first session and test session of the bow tie maze task. Rats (n = 10 for all groups) with NRe lesions (“Lesion”) or sham lesions (“Sham”) underwent training in the bow tie maze task, where they were exposed to novel or familiar objects. The discrimination ratio D2 (+/- s.e.m.) is shown for performance in the first session and in the test session of the task. Significance: * $p < 0.05$, ** $p < 0.01$, *** $p < 0.001$.

All rats showed similar levels of cumulative exploration in the first session of the bow tie maze (Figure 3.3). Exploration times were generally reduced in the test session, and overall lower for the rats that had explored highly familiar objects (Figure 3.3). Repeated measures ANOVA showed no significant main effects of session ($F(1,36) = 0.522$, $p = 0.475$), type of stimulus ($F(1,36) = 1.440$, $p = 0.281$) or surgical procedure ($F(1,36) = 1.198$, $p = 0.281$) and no interaction effect ($F(1,36) = 0.377$, $p = 0.543$). Overall, the NRe lesion did not affect the rats' ability to explore objects.

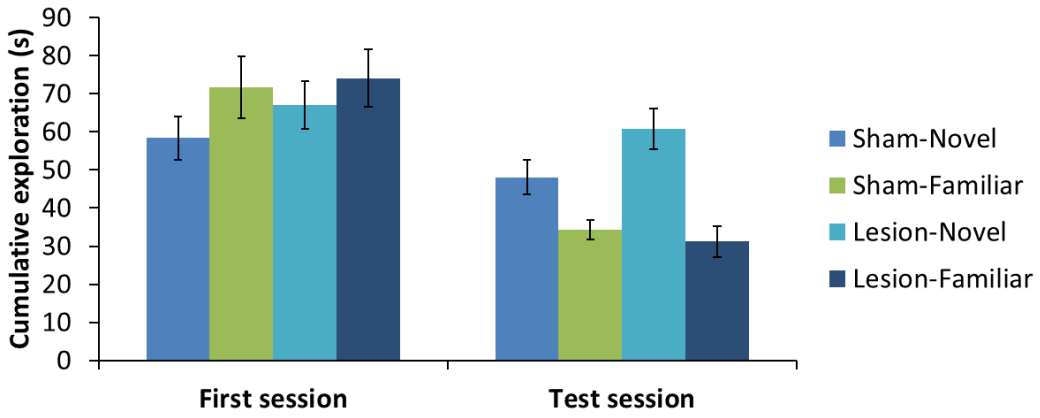

Figure 3.3: Cumulative exploration in the first session and the test session of the bow tie maze task. Exploration (in seconds +/- s.e.m.) is shown for rats with NRe lesions ("Lesion") or sham lesions ("Sham") during exploration of novel or highly familiar objects (n = 10 for all groups).

3.3. c-fos expression in the recognition memory network: frequentist approach

Levels of the immediate early gene c-fos were measured in several brain regions associated with the recognition memory network 90 minutes after the test session of the bow tie maze task.

No differences in mean counts of Fos positive nuclei in the prefrontal cortex areas prelimbic cortex (PRL), infralimbic cortex (IFC), anterior cingulate cortex (ACC), ventral orbital cortex (VOC) or medial orbital cortex (MOC), were detected between any of the four experimental groups (Figure 3.4).

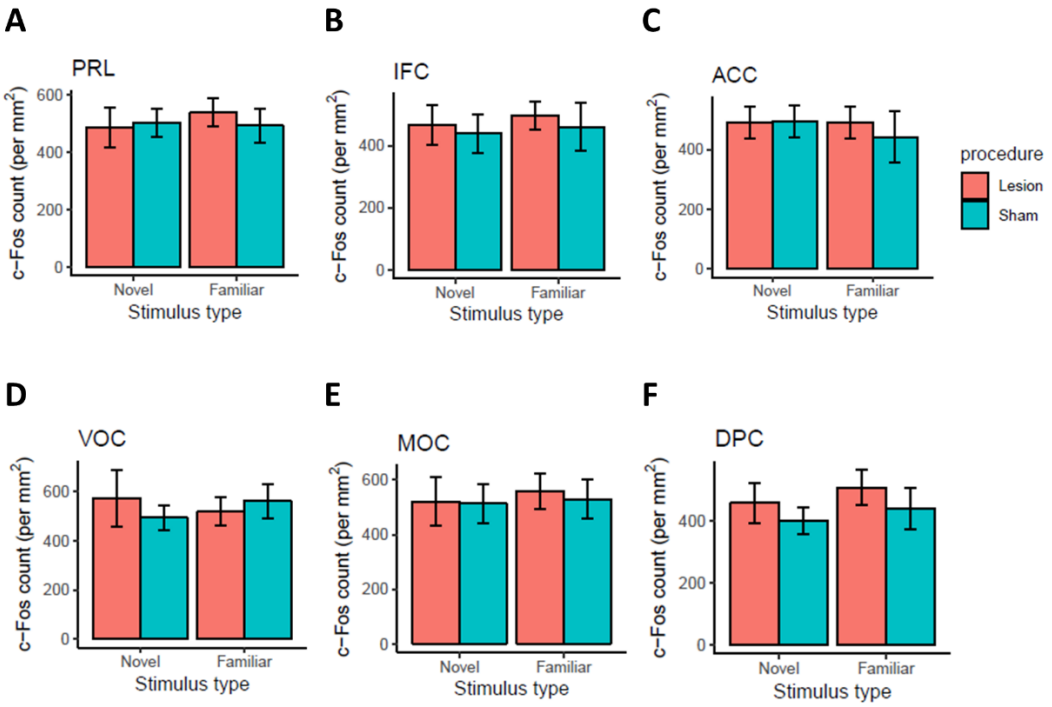

Figure 3.4: c-fos counts in the prefrontal cortex following the bow tie maze task. Levels of Fos were measured in NRe-lesioned and sham lesioned rats, 90 min after exposure to novel and familiar objects in the bow tie maze task (n = 10 for each group). Mean counts of Fos positive cells per mm^2 (+/- s.e.m) are shown for (A) prelimbic cortex (PRL), (B) infralimbic cortex (IFL), (C) anterior cingulate cortex (ACC), (D) ventral orbital cortex (VOC), (E) medial orbital cortex (MOC), (F) dorsal peduncular cortex (DPC).

Two-way ANOVA showed no significant main effects of stimulus type (novel vs familiar; PRL: $F(1,34) = 0.127$, $p = 0.724$; IFC: $F(1,32) = 0.158$, $p = 0.694$; ACC: $F(1,33) = 0.161$, $p = 0.691$; VOC: $F(1,31) = 0.002$, $p = 0.965$; MOC: $F(1,29) = 0.127$, $p = 0.724$) and no main effects of surgical procedure (sham vs lesion; PRL: $F(1,34) = 0.084$, $p = 0.774$; IFC: $F(1,32) = 0.269$, $p = 0.608$; ACC: $F(1,33) = 0.131$, $p = 0.720$; VOC: $F(1,31) = 0.0064$, $p = 0.802$; MOC: $F(1,29) = 0.064$, $p = 0.803$). There were also no significant stimulus x procedure interactions (PRL: $F(1,34) = 0.296$, $p = 0.590$; IFC: $F(1,32) = 0.004$, $p = 0.950$; ACC: $F(1,33) = 0.189$, $p = 0.667$; VOC: $F(1,31) = 0.617$, $p = 0.438$; MOC: $F(1,29) = 0.0.021$, $p = 0.887$). In the dorsal peduncular cortex (DPC) (Figure 3.4), Fos levels appeared to be elevated in NRe-lesioned rats compared to sham rats, but this effect was not statistically significant (main effect of stimulus: $F(1,32) = 0.554$, $p = 0.462$; main effect of procedure: $F(1,32) = 1.13$, $p = 0.296$; stimulus x procedure interaction: $F(1,32) = 0.009$, $p = 0.926$)

In conclusion, neither the type of stimulus the rats explored, nor the NRe lesion appeared to affect Fos levels in the prefrontal cortex.

Levels of Fos in dorsal, intermediate and ventral hippocampal subregions are depicted in Figure 3.5. In the CA1 subregion of the dorsal hippocampus, Fos levels were non-significantly higher in Sham-Familiar rats compared to the other groups (main effect of stimulus: $F(1,28) = 0.483$, $p = 0.493$; main effect of procedure: $F(1,28) = 0.634$, $p = 0.433$; interaction effect: $F(1,28) = 0.652$; $p = 0.426$). In intermediate and ventral CA1 (ICA1, VCA1), a similar pattern of c-fos expression was observed, where levels of Fos were higher in Sham-Novel compared to Sham-Familiar, while c-fos expression in the lesion group appeared unaffected by stimulus type. However, the observed differences were not statistically significant (main effect of stimulus – ICA1: $F(1,21) = 0.678$, $p = 0.420$; VCA1: $F(1,25) = 1.02$, $p = 0.322$; main effect of procedure – ICA1: $F(1,21) = 0.019$, $p = 0.893$; VCA1: $F(1,25) = 0.069$, $p = 0.795$; interaction effect – ICA1: $F(1,21) = 0.476$, $p = 0.498$; VCA1: $F(1,25) = 2.29$, $p = 0.143$).

No significant differences between any of the groups were detected in dorsal CA3 (main effect of stimulus: $F(1,31) = 0.458$, $p = 0.504$; main effect of procedure: $F(1,31) = 0.804$, $p = 0.377$; interaction effect: $F(1,31) = 0.016$, $p = 0.900$). In the intermediate CA3, c-fos counts appeared to be higher in the lesion groups compared to the sham groups, in particular when the rats were shown familiar objects, although this effect was not significant (main effect of stimulus: $F(1,22) = 0.242$, $p = 0.627$; main effect of procedure: $F(1,22) = 0.637$, $p = 0.433$; interaction effect: $F(1,22) = 0.143$, $p = 0.209$). Ventral CA3 (VCA3) Fos levels were generally non-significantly increased in the NRe-lesioned rats compared to sham rats, irrespective of the object type shown (main effect of stimulus: $F(1,22) = 0.847$, $p = 0.367$; main effect of procedure: $F(1,22) = 2.66$, $p = 0.117$; interaction effect: $F(1,22) = 0.190$, $p = 0.668$).

In dorsal dentate gyrus (DDG) and ventral dentate gyrus (VDG), no significant differences in Fos levels were observed (main effect of stimulus – DDG: $F(1,29) = 0.268$, $p = 0.608$; VDG: $F(1,22) = 0.159$, $p = 0.694$); main effect of procedure – DDG: $F(1,29) = 0.578$, $p = 0.453$; VDG: $F(1,22) = 0.519$, $p = 0.479$; interaction effect – DDG: $F(1,29) = 0.002$, $p = 0.962$; VDG: $F(1,22) = 0.305$, $p = 0.586$). Sham-Familiar rats showed a non-significant reduced c-fos count in the intermediate dentate gyrus, compared to the other groups (main effect of stimulus: $F(1,19) = 1.31$, $p = 0.267$; main effect of procedure: $F(1,19) = 1.09$, $p = 0.309$ interaction effect: $F(1,19) = 0.381$, $p = 0.544$).

In dorsal subiculum (DSUB), no substantial differences in c-fos expression were detected between the experimental groups (main effect of stimulus: $F(1,16) = 1.30$, $p = 0.272$; main effect of procedure: $F(1,16) = 0.312$, $p = 0.584$; interaction effect: $F(1,16) = 0.379$, $p = 0.547$). A c-fos expression pattern similar to the one in ICA1 and VCA1 was observed in the ventral subiculum (VSUB), i.e. overall higher c-fos counts in the Sham-Novel group and overall lower counts in the Sham-Familiar group. These differences in Fos levels were not statistically significant (main

effect of stimulus: F(1,19) = 2.12, p = 0.162; main effect of procedure: F(1,19) = 0.336, p = 0.569; interaction effect: F(1,19) = 2.81, p = 0.110).

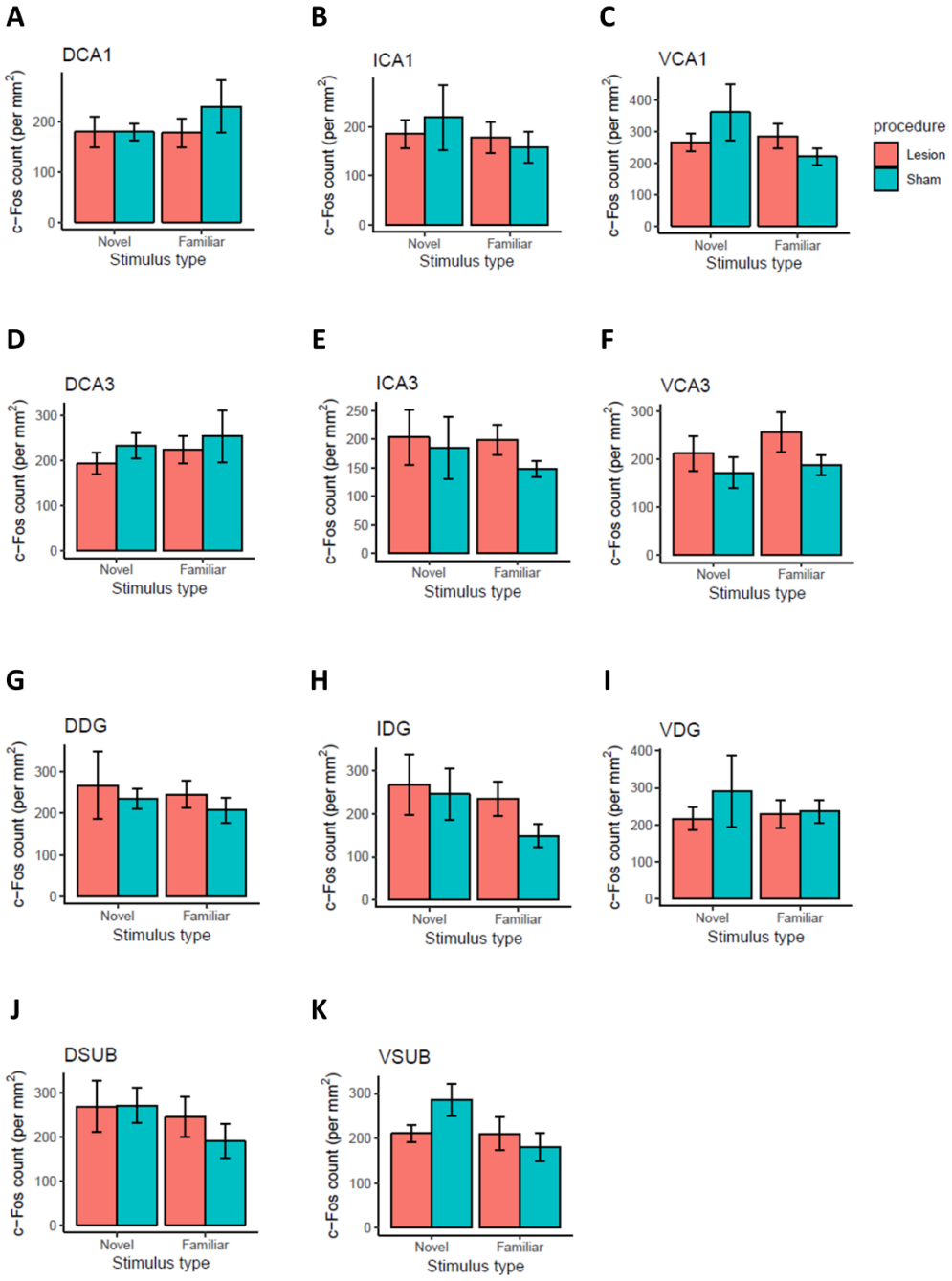

Figure 3.5: c-fos counts in the hippocampal formation following the bow tie maze task. Levels of c-fos were measured in NRe-lesioned and sham lesioned rats, 90 min after exposure to novel and familiar objects in the bow tie maze task (n = 10 for each group). Mean counts of c-fos positive cells per mm^2 (+/- s.e.m) are shown for (A) dorsal CA1, (B) intermediate CA1 (ICA1), (C) ventral CA1 (VCA1), (D) dorsal CA3 (DCA3), (E) intermediate CA3 (ICA3), (F) ventral CA3 (VCA3), (G) dorsal dentate gyrus (DDG), (H) intermediate dentate gyrus (IDG), (I) ventral dentate gyrus (VDG), (J) dorsal subiculum (DSUB), (K) ventral subiculum (VSUB). Significance: ** $p < 0.01$.

Mean counts of Fos positive nuclei in areas of the rhinal cortex are depicted in Figure 3.6. Like subfields of the hippocampus, a pattern of c-fos expression was detected in the perirhinal cortex (PRH) and the temporal association cortex (TE2) which showed increased levels of Fos in sham rats exposed to novel objects compared to those exposed to familiar, while NRe lesioned rats did not show any such effect of object type. The observed differences were not significant in the PRH (main effect of stimulus: $F(1,32) = 0.731$, $p = 0.399$; main effect of procedure: $F(1,32) = 0.555$, $p = 0.462$; interaction effect: $F(1,32) = 1.694$, $p = 0.202$). In the TE2, the main effect of stimulus type and the stimulus x procedure interaction were not significant, but the *p* value was close to 0.05 (main effect of stimulus: $F(1,34) = 3.74$, $p = 0.062$; main effect of procedure: $F(1,34) = 0.145$, $p = 0.706$; interaction effect: $F(1,34) = 3.92$, $p = 0.056$). No significant differences between the different experimental groups in levels of Fos were observed in postrhinal cortex (PSTC) or lateral entorhinal cortex (LENT) (main effect of stimulus – PSTC: $F(1,30) = 1.18$, $p = 0.287$; LENT: $F(1,28) = 0.158$, $p = 0.694$; main effect of procedure – PSTC: $F(1,30) = 0.039$, $p = 0.845$; LENT: $F(1,28) = 0.316$, $p = 0.579$; interaction effect – PSTC: $F(1,30) = 0.048$, $p = 0.828$; LENT: $F(1,28) = 0.385$, $p = 0.540$).

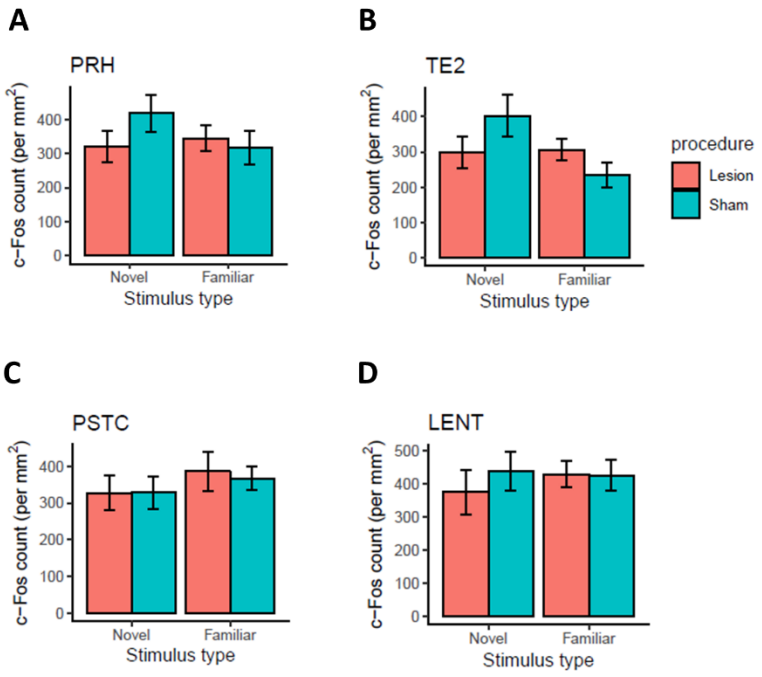

Figure 3.6: c-fos counts in the rhinal cortex following the bow tie maze task. Levels of Fos were measured in NRe-lesioned and sham lesioned rats, 90 min after exposure to novel and familiar objects in the bow tie maze task (n = 10 for each group). Mean counts of Fos positive cells per mm^2 (+/- s.e.m) are shown for (A) perirhinal cortex (PRH), (B) TE2, (C) postrhinal cortex (PSTC), (D) lateral entorhinal cortex (LENT).

Levels of Fos in the motor cortex M2 and visual cortex V2 were measured as control regions, in which we did not expect to see changes in Fos levels in response to object exploration (Figure

3.7). Two-way ANOVA revealed no significant differences in Fos counts in the motor cortex (main effect of stimulus: F(1,32) = 0.029, p = 0.867; main effect of procedure: F(1,32) = 0.004, p = 0.953; interaction effect: F(1,32) = 0.055, p = 0.817) or the visual cortex (main effect of stimulus: F(1,30) =0.002, p = 0.964; main effect of procedure: F(1,30) = 0.452, p = 0.507; interaction effect: F(1,30) = 1.57, p = 0.220).

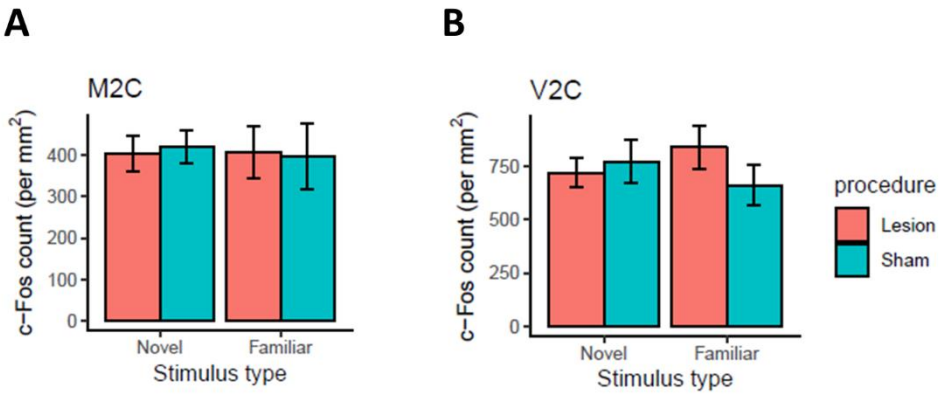

Figure 3.7: c-fos counts in the motor and visual cortex following the bow tie maze task. Levels of Fos were measured in NRe-lesioned and sham lesioned rats, 90 min after exposure to novel and familiar objects in the bow tie maze task (n = 10 for each group). Mean counts of c-fos positive cells per mm^2 (+/- s.e.m) are shown for (A) motor cortex M2, (B) visual cortex V2C.

Taken together, while statistical analysis of Fos positive cells in brain regions of the recognition memory network following the bow tie maze task indicated no significant effects of stimulus type or surgical procedure on Fos levels, non-significant differences between of Fos counts were observed for several hippocampal subfields, perirhinal cortex and area TE2.

3.4. c-fos expression in the recognition memory network: Bayesian approach

In addition to the standard frequentist statistical analysis described in section 3.3, counts of Fos positive cells were analysed using Bayesian hierarchical modelling. For each brain region and experimental group, the Bayesian analysis produced 4000 theta samples and one estimated mean theta value. With four experimental groups and 23 analysed brain regions, a total of 92 mean theta values and respective sample sets were generated.

Mean theta values per brain region are shown in Figure 3.8 for each experimental group. Differences in mean theta values between experimental groups were apparent in hippocampal subregions, in particular ICA1, ICA3 and IDG, along with VCA1, VCA3 and VSUB. Differences were also observed infralimbic cortex, perirhinal cortex and area TE2.

For each brain region, differences in theta values between the different experimental groups were analysed using Null Hypothesis Significance Testing (Table 3.1). As suggested by the visual differences in Figure 3.8, significant differences were mainly focussed on hippocampal subfields IDG, ICA3, VCA3, VSUB, PRH and TE2. The P(group1>group2) column shows the probability that theta of group 1 is bigger than theta of group 2. Extreme values (i.e. very small or very large probabilities) further supported the hypothesis that there was a significant difference between the two thetas.

Figure 3.8: (Next page) Mean theta values per brain region. Estimated mean theta values per brain region for each experimental group are shown. Values were transformed back to the original scale of the experimental data (Fos counts) before plotting.

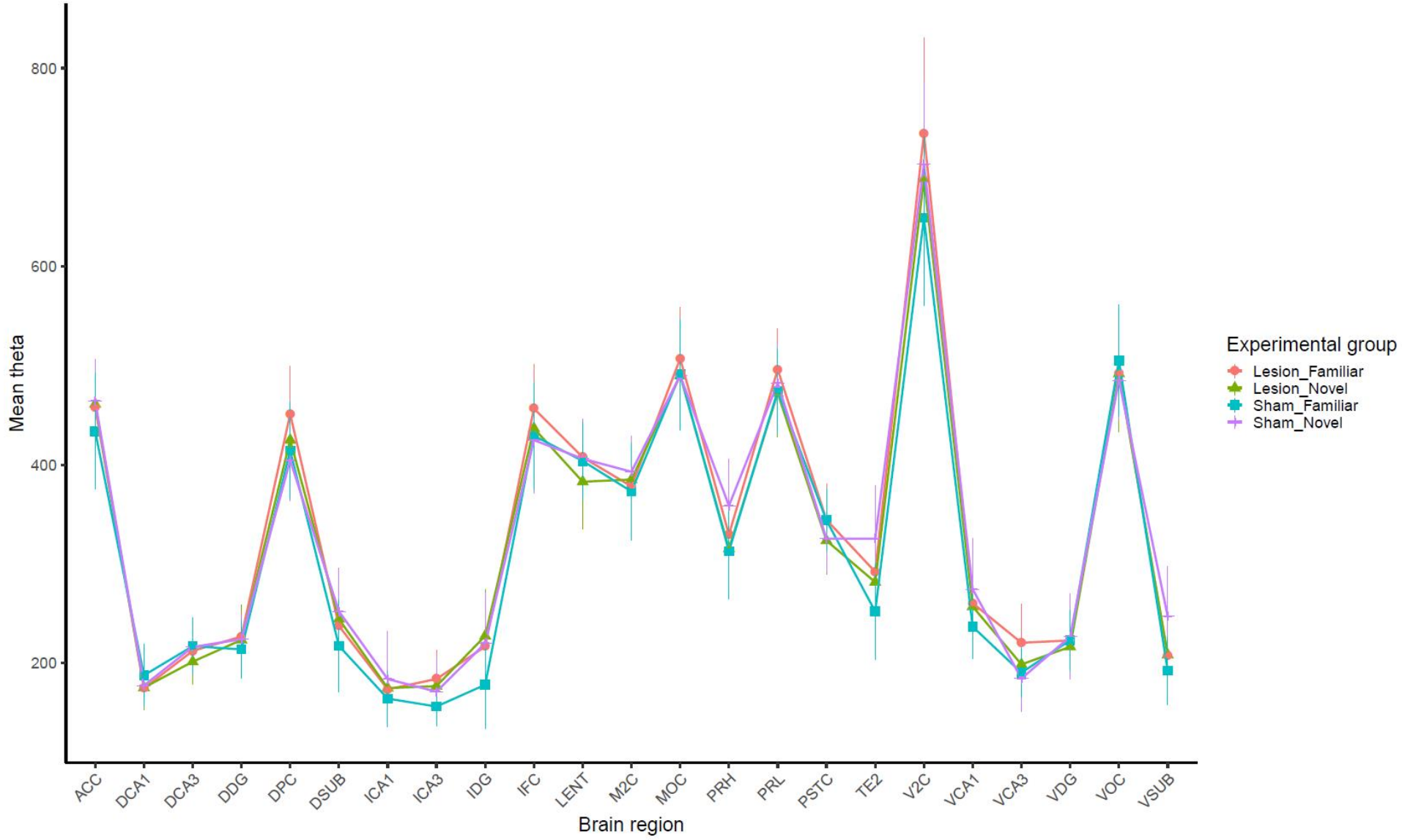
Mean theta
800
600
400
200
ACC
DCA1
DCA3
DDG
DPC
DSUB
ICA1
ICA3
IDG
IFC
LENT
M2C
MOC
PRH
PRL
PSTC
TE2
V2C
VCA1
VCA3
VDG
VOC
VSUB
Brain region
Experimental group
Lesion_Familiar
Lesion_Novel
Sham_Familiar
Sham_Novel

Table 3.1: Significant differences between experimental groups. Estimated mean theta values were compared pair-wise by Null Hypothesis Significance Testing (pval). The P(group1>group2) column shows the probability that theta of Group 1 is bigger than theta of Group 2.

Brain region	Group 1	Group 2	pval	P(group1>group2)
TE2	Sham_Novel	Sham_Familiar	0.00863	0.8425
VSUB	Sham_Novel	Sham_Familiar	0.01317	0.8365
IDG	Lesion_Novel	Sham_Familiar	0.02547	0.813
ICA3	Lesion_Familiar	Sham_Familiar	0.02586	0.8105
DPC	Lesion_Familiar	Sham_Novel	0.03632	0.78625
VCA3	Lesion_Familiar	Sham_Novel	0.03949	0.78425
IDG	Lesion_Familiar	Sham_Familiar	0.0413	0.784
TE2	Lesion_Familiar	Sham_Familiar	0.04425	0.78025
VSUB	Lesion_Novel	Sham_Novel	0.04464	0.21875
PRH	Lesion_Novel	Sham_Novel	0.04756	0.2325

Figure 3.9 A-C shows the overlapping theta density plots for the top three significant differences shown in Table 3.1. As a comparison, overlapping plots of three theta pairs that are least different from each other are shown, defined by a probability of approximately 0.5 of one theta being larger than the other (Figure 3.9 D-F).

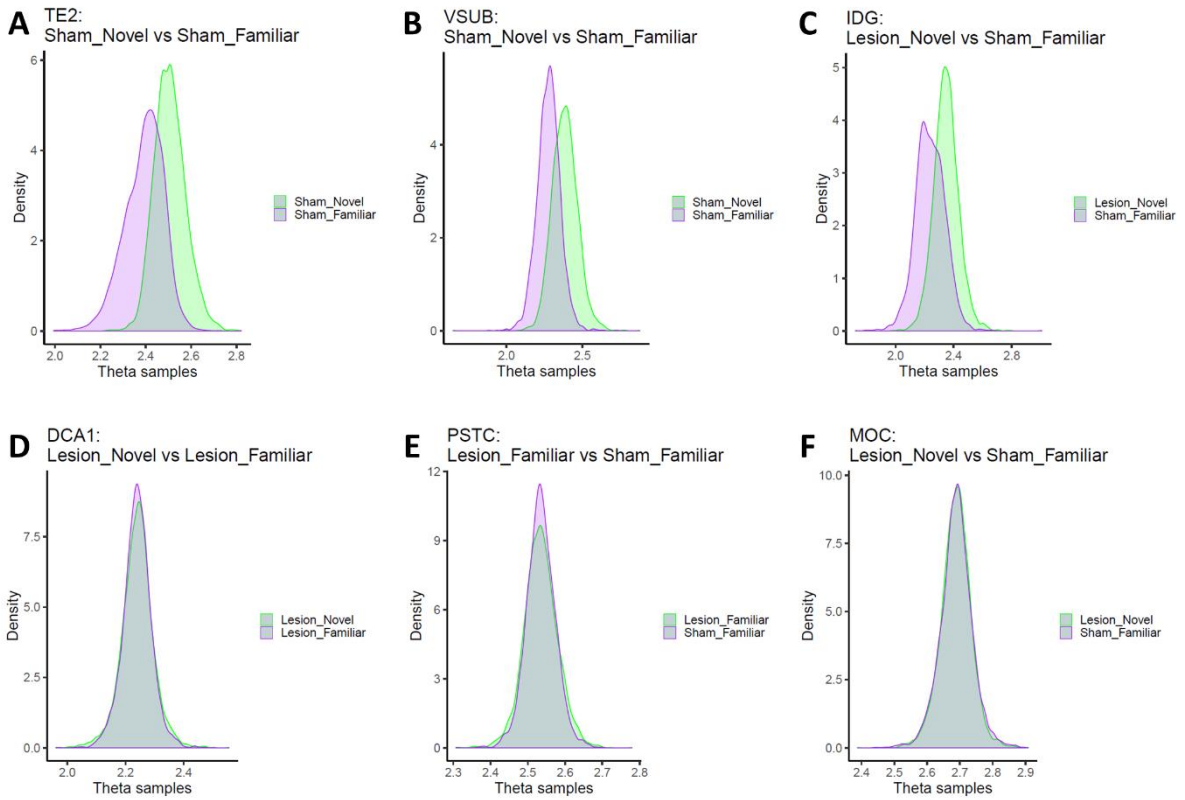

Figure 3.9: Pairwise comparisons of theta samples. Theta samples for two thetas are presented as density plots. (A) Sham-Novel vs Sham-Familiar in TE2 (P(Sham-Novel > Sham-Familiar) = 0.843), (B) Sham-Novel vs Sham-Familiar in ventral subiculum (P(Sham-Novel > Sham-Familiar) = 0.837), (C) Lesion-Novel vs Sham-Familiar in intermediate dentate gyrus (P(Lesion-Novel > Sham-Familiar) = 0.813), (D) Lesion-Novel vs Lesion-Familiar in dorsal CA1 (P(Lesion-Novel > Lesion-Familiar) = 0.500), (E) Lesion-Familiar vs Sham-Familiar in postrhinal cortex (P(Lesion-Familiar > Sham-Familiar) = 0.498), (F) Lesion-Novel vs Sham-Familiar in medial orbital cortex (P(Lesion-Novel > Sham-Familiar) = 0.503).

Taken together, the Bayesian analysis results suggest that there are significant differences in Fos levels in hippocampal subfields, PRH and TE2, both when comparing the type of stimulus the rats were exposed to and the type of lesion.

3.5. Comparison between Bayesian and frequentist analysis

As shown in Figure 3.10, the partial pooling employed in the Bayesian model, which assumes that counts from all animals and groups are governed by a joint distribution, pulled the estimated mean theta values closer together compared to the sample means determined by frequentist statistics.

Linear regression analysis provided a fit line with a slope of 0.952 (standard error +/- 0.018) which was significantly different of the diagonal slope of 1 ($t(90) = -2.73$, $p = 0.008$), suggesting that the spread of the Bayesian values and frequentist values was not equivalent.

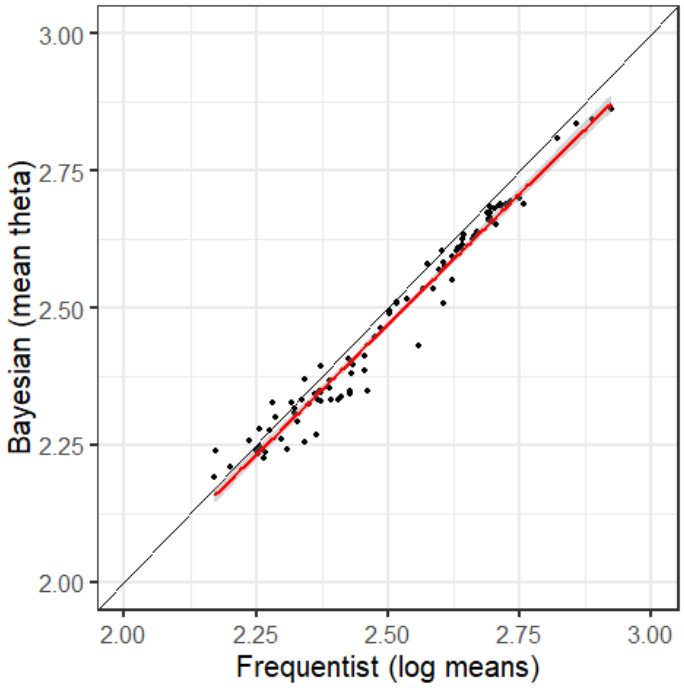

Figure 3.10: Comparing the spread of estimated mean theta values and frequentist sample means. Mean theta values estimated through Bayesian modelling, are plotted against their corresponding frequentist log-transformed sample means. One value per brain region per experimental group is shown. A linear regression line (in red, associated standard error in grey) was fitted to the data points. The diagonal is marked in black.

For further comparison of frequentist and Bayesian approaches, a simulated data set was generated from the posterior probability distribution for each theta that had been estimated through Bayesian modelling of the experimental data. Sample means determined by standard frequentist statistics and mean theta values estimated through Bayesian analysis of this simulated data set were plotted against their respective standard errors (Figure 3.11). As with comparison of the two approaches using the experimental data set, Bayesian estimates were pulled towards the global mean, compared to the frequentist sample means. Furthermore, standard errors were overall lower when using the Bayesian approach, in particular for means that had been associated with high standard errors when using frequentist analysis. The results suggest that Bayesian mean estimates are associated with lower uncertainty than frequentist sample means.

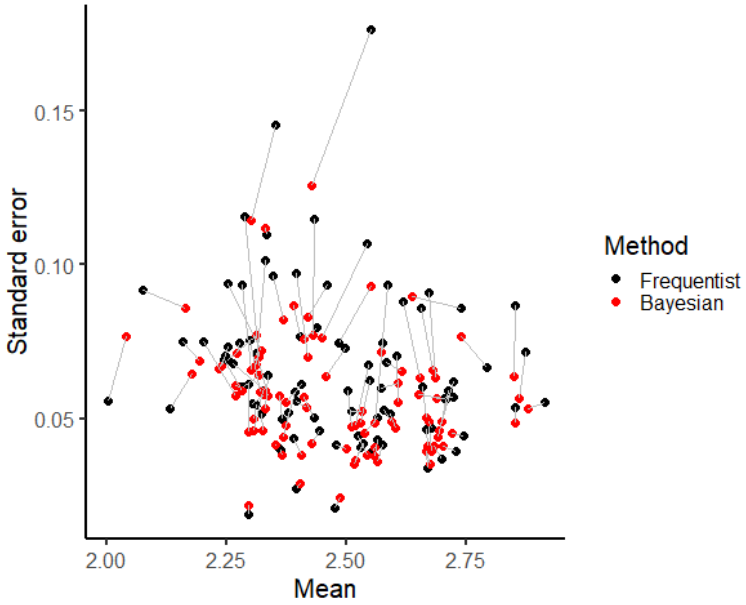

Figure 3.11: Comparing the means and standard errors of frequentist and Bayesian approaches. For each brain region and experimental group, mean log cell counts determined either by standard frequentist statistics (black) or Bayesian hierarchical modelling (red) of a simulated data set were plotted against their standard errors.

Next the simulated data sets were used to investigate how accurately Bayesian and frequentist statistics estimate the true mean of a population. The true mean of the simulated data can be defined as the original theta values, estimated from the experimental data. By using both frequentist statistics and Bayesian modelling on the simulated data set, we can compare the resulting sample means and theta values to the true means to quantify the accuracy of both methods. Calculation of the mean sum squared error of the calculated frequentist means and estimated Bayesian thetas compared to the true means, using ten separate simulated sample sets, indicated that Bayesian modelling provided mean estimates with a 54% lower error compared to the frequentist approach (Figure 3.12).

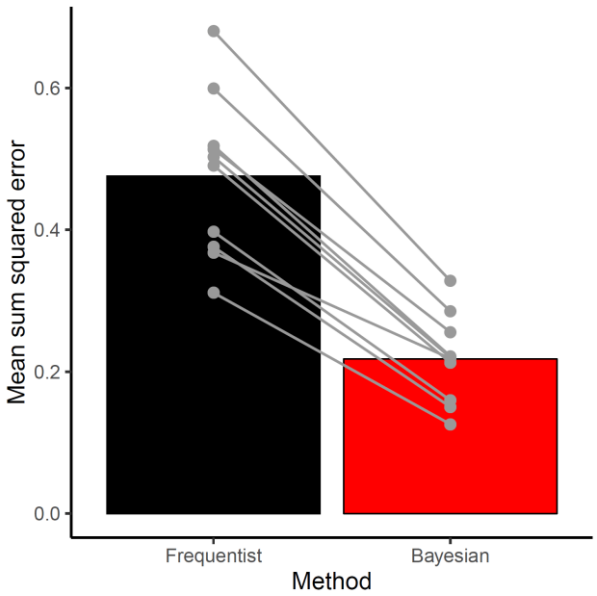

Figure 3.12: Comparison of the error associated with Bayesian and frequentist statistics. The sum squared error of the Bayesian estimated mean theta values and frequentist sample means from the true mean of a simulated data set was calculated for 10 iterations. The mean sum squared error along with the individual sum squared error values for each iteration are shown for both statistical approaches.

Together the results suggested that mean cell counts estimated through Bayesian modelling were associated with lower uncertainty and higher accuracy than sample means calculated by standard frequentist statistics.

4. Discussion

4.1. The NRe is not required for object recognition memory in the bow-tie maze task

Rats with NRe lesions were able to perform in the bow-tie maze task as well as sham lesioned rats, which suggests that the NRe is not required for recognition memory performance in this task. The bow-tie maze task is considered a paradigm that tests the single-item memory of the rat, i.e. its ability to discriminate between a novel object and a familiar object (Albasser *et al*., 2010). While some rats showed only partial lesioning of the NRe, which could reduce potential behavioural effects of the NRe lesion, the present results are in line with previous research which showed that lesions of the NRe did not impair recognition memory for single items in the spontaneous object recognition task (Barker and Warburton, 2018), whereas associative recognition memory was disrupted (Barker and Warburton, 2018). Single-item recognition memory is thought to rely on the perirhinal cortex (Ennaceur *et al*., 1996; Bussey *et al*., 1999; Wan *et al*., 1999; Barker *et al*., 2007; Barker and Warburton, 2011) and not the mPFC (Mitchell and Laiacona, 1998; Barker *et al*., 2007), while involvement of the HPC is disputed (Clark *et al*., 2000; Bussey *et al*., 2000; de Lima *et al*., 2006; Winters *et al*., 2004; Barker and Warburton, 2011; Albasser *et al*., 2012). Therefore, the observation that NRe lesions don't affect single-item recognition memory further supports the hypothesis that the NRe is only directly required for the formation of memories that involve communication between the HPC and the mPFC or for tasks with a higher mnemonic demand.

The performance of NRe lesioned rats and sham rats in the bow-tie maze task also allowed assessment of whether the rats in group familiar had been familiarised to the repeatedly explored objects. The lack of discrimination between the object pairs by the group familiar rats in the test session indicated that these rats had encoded and were familiar with the objects. Therefore, the subsequent histological analysis allows comparison of Fos levels between rats that explored novel objects and those that explored highly familiar objects.

4.2. Bayesian analysis outperformed standard frequentist statistics

Gene expression of c-fos in the various brain regions of the recognition memory network was analysed using both standard frequentist statistics and Bayesian hierarchical modelling. Comparison of Bayesian and frequentist analysis of a simulated data set suggested that the Bayesian approach outperformed the standard frequentist statistics. Due to use of a simulated data set, it was possible to compare the mean values determined by frequentist statics and the equivalent theta values estimated by Bayesian modelling with the true mean of the population.

Comparison of the sum squared errors between the two statistical approaches indicated that the Bayesian method produced estimated values closer to the true mean and was therefore an improvement over the frequentist approach.

Bayesian analysis allowed inclusion of the experimental hierarchy through the use of partial pooling. This approach which was expected to be useful for the Fos data obtained from the bow-tie maze experiment, as *in vivo* experiments can be associated with high variability between rats, occasional missing values due to varying tissue and staining quality, and low replicate number due to the limitation of experimentation using animals. By pulling the individual estimates towards a group and global mean, partial pooling was able to reduce the uncertainty in the data, mitigate high levels of variability between animals and provide estimates for missing data. Moreover, Bayesian modelling produces posterior probability distributions for each estimated parameter, enabling assessment of the uncertainty associated with the generated model.

While implementation of the code required for the Bayesian modelling approach took longer than the use of standard frequentist statistics, the above-mentioned advantages over the frequentist approach suggest Bayesian analysis as a useful statistical tool for analysis of data obtained from in vivo experiments, as described here.

4.3. NRe lesion affected c-fos expression in the recognition memory network

While the NRe did not appear to contribute directly to performance in the bow-tie maze task to an extent that the rats were unable to successfully discriminate between the objects, it is still possible that the NRe modulates neural activity in other brain regions of the recognition memory network that it is directly or indirectly connected to.

Immediate early gene c-fos is considered an indicator of neuronal activity. Its expression is transiently induced within 90 min of neuronal activation and, as a transcription factor, Fos activates the expression of late response genes important for memory formation. Previous studies using the bow tie maze have reported altered c-fos expression in hippocampal subfields that can be lesioned without affecting performance in the task (Albasser *et al*., 2010). Even though these brain regions are not essential for the task, they may still encode associative information about the object's environment that is not needed for this specific task. This makes the bow-tie maze a useful paradigm for studying neural activity within the recognition memory network not limited to brain regions directly involved in single-item recognition memory.

In the present study, c-fos expression was analysed in multiple brain regions of the recognition memory network in sham and NRe lesioned rats, in response to exploring novel or familiar

objects. Analysis of Fos levels by frequentist statistics did not uncover any significant differences between experimental groups in any brain regions, although non-significant effects of lesion type and stimulus on Fos levels were observed in hippocampal subfields, perirhinal cortex and area TE2.

Pair-wise comparison of estimated mean theta values, which are the Bayesian equivalent of sample means calculated in frequentist statistics, using Null Hypothesis Significance Testing indicated significant differences in Fos levels in subfields of the hippocampus, perirhinal cortex, TE2 and dorsal peduncular cortex. These differences were further supported by high probability levels of one mean theta value being larger than the other for all significantly different theta pairs.

A significant impact of object type, i.e. exploration of novel versus highly familiar object, was observed for sham rats in area TE2 and ventral subiculum. Higher Fos levels in area TE2 of rats exploring novel objects compared to those exploring familiar objects was previously reported in the bow-tie maze task (Albasser *et al*., 2010). Furthermore, it has been shown that lesioning of the TE2 impaired object recognition memory when delays between the sample and test phase were 20 minutes or longer (Ho *et al*., 2011), suggesting that the TE2 may be required for the performance in the bow tie maze task.

A common observation following exposure to novel objects is the induction of c-fos expression in the perirhinal cortex. Rats subjected to paired-viewing experiments consistently showed increased Fos protein in the perirhinal cortex associated with viewing a novel object (Zhu *et al*., 1995, Zhu *et al*., 1996, Wan *et al*., 1999). In the present study, neither sham rats nor NRe-lesioned rats showed differential c-fos expression in response to novel versus familiar stimuli. Previous studies involving the bow-tie maze produced contrasting results. One study found increased levels of c-fos expression in the caudal perirhinal cortex of rats that had explored novel objects compared to familiar objects (Albasser *et al*., 2010). In line with the present results, Kinnavane *et al*. observed no significant differences in Fos levels in either area 35 or 36 of the caudal perirhinal cortex of sham lesioned rats, following the bow-tie maze task (Kinnavane *et al*., 2014). Notably, there is a critical difference between the paired viewing task and the bow-tie maze task. In the paired viewing task, rats view a novel image with one eye and a familiar image with the other. Therefore c-fos expression can be directly linked to exposure to the novel or the familiar stimulus. In contrast, in the bow-tie maze task there is no such ‘within-rat’ comparison of c-fos expression. Instead, the group Novel rats are required to make several familiarity discriminations between one entirely novel object and one object that has just been seen for the first time on the previous trial. It has been suggested that c-fos expression in the Novel rats may therefore be a measure of familiarity, rather than of novelty and thus not

necessarily be associated with an increase in Fos levels in the perirhinal cortex (Kinnavane *et al*., 2014).

It was, however observed, that rats with sham lesions had significantly higher Fos levels in the perirhinal cortex than those with NRe lesions when exposed to novel objects. Similar effects of the NRe lesion were observed in intermediate CA3, intermediated dentate gyrus ventral subiculum and TE2. Furthermore, in some brain regions the counts of Fos-positive nuclei were affected by both lesion and stimulus type. In the intermediate dentate gyrus, there was a higher level of c-fos expression in the Lesion-Novel compared to the Sham-Familiar group, while in the dorsal peduncular cortex and the ventral CA3 higher levels were observed in Lesion-Familiar compared to Sham-Novel.

The NRe has direct projections to the perirhinal cortex, entorhinal cortex and subfields of the medial prefrontal cortex and hippocampus (Wouterlood *et al*., 1990; Vertes, 2002; McKenna and Vertes, 2004; Vertes *et al*., 2006; Hoover and Vertes, 2012). It could be argued that lesioning of any brain region would lead to the loss of excitatory inputs into directly connected brain regions. Therefore, any observed reductions in c-fos expression in the present experiment could be explained by a general lesion-effect, independent of the actual lesion site. In contrast, while the NRe selectively targets CA1 and subiculum, it is not directly connected to CA3 or dentate gyrus (Wouterlood *et al*., 1990; Vertes *et al*., 2006). Yet in the present study, NRe lesions affected levels of Fos in intermediate CA3 and dentate gyrus, in addition to TE2 and dorsal peduncular cortex. This suggests that the observed effects of the lesion on c-fos expression in the recognition memory network are more likely true functional effects specifically of lesioning the NRe.

4.4. Conclusion and future directions

The present study provides further evidence that the NRe is not required for single-item recognition memory. Nevertheless, use of Bayesian analysis showed that lesioning of the NRe led to changes in c-fos expression in several brain regions of the recognition memory network. This supports the hypothesis that the NRe may have a supportive or modulatory function by providing a relay point in the recognition memory network for information flow between brain regions.

The precise role of the NRe within the recognition memory network remains to be defined. Electrophysiological studies may shed further light on how and when the NRe modulates neural activity within interconnected brain regions of the memory circuit. Considering that differences in c-fos expression following the NRe lesion were also observed in regions other than HPC and

mPFC, it will be of interest to explore how the NRe contributes to information flow between other nodes of the recognition memory network, outside of the HPC-NRe-mPFC subcircuit.

Additionally, while the Bayesian approach has shown benefits over standard statistical modelling, steps could be taken to potentially further improve the generated Bayesian model. In the current study, Bayesian testing was run using an empirical prior, i.e. the mean of the prior distribution was based on the global sample mean of the measured counts of Fos-positive cells obtained in the present bow tie maze experiment. A further advantage of Bayesian modelling is that it can re-use previously published data by basing the prior on previous data. This means that the generated model can also be further refined by the addition of additional data and the resulting hypotheses strengthened.

The presented Bayesian analysis assumed that all brain region counts were independent, apart from the partial pooling that was applied. However, the brain regions are in fact interconnected as part of the recognition memory network, meaning that Fos levels in one brain region is likely to influence Fos levels in other regions. Future analysis will utilise the existing data set to establish a Bayesian hierarchical model which assumes that the brain regions are not independent and can therefore estimate correlations between brain regions. The results from this analysis will enable further understanding of the information flow between the different brain regions in the recognition memory network in normal animals and those without a functional NRe.

Finally, now that a Bayesian model has been established, this can further be used to generate hypotheses for future practical experiments, for example by lesioning brain regions in silico and examining expected results.

References

Albasser MM, Amin E, Lin TC, Iordanova MD, Aggleton JP (2012) Evidence that the rat hippocampus has contrasting roles in object recognition memory and object recency memory. Behav Neurosci 126:659-669

Albasser MM, Poirier GL, Aggleton JP (2010) Qualitatively different modes of perirhinal-hippocampal engagement when rats explore novel vs. familiar objects as revealed by c-Fos imaging. Eur J Neurosci 31: 134-47.

Barker GRI, Banks PJ, Scott H, Ralph GS, Mitrophanous KA, Wong LF, Bashir ZI, Uney JB, Warburton EC (2017) Separate elements of episodic memory subserved by distinct hippocampal-prefrontal connections. Nat Neurosci 20: 242-50.

Barker GRI, Bird F, Alexander V, Warburton EC (2007) Recognition memory for objects, place and temporal order: A disconnection analysis of the role of the medial prefrontal cortex and perirhinal cortex. J Neurosci 27: 2948-57.

Barker GRI, Warburton EC (2011) When is the hippocampus involved in recognition memory? J Neurosci 31:10721-31

Barker GRI, Warburton EC (2018) A critical role for the nucleus reuniens in long-term, but not short-term associative recognition memory formation. J Neurosci pii: 1802-17. doi: 10.1523/JNEUROSCI.1802-17.2017. [Epub ahead of print]

Bullit E (1990) Expression of C-fos-like protein as a marker for neuronal activity following noxious stimulation in the rat. J Comp Neurol 296:517-30.

Bussey TJ, Dias R, Amin E, Muir JL, Aggleton JP (2001) Perirhinal cortex and place-object conditional learning in the rat. Behav Neurosci 115:776-85.

Bussey TJ, Duck J, Muir JL, Aggleton JP (2000) Distinct patterns of behavioural impairments resulting from fornix transection or neurotoxic lesions of the perirhinal and postrhinal cortices in the rat. Behav Brain Res 111:187-202.

Bussey TJ, Muir JL, Aggleton JP (1999) Functionally dissociating aspects of event memory: the effects of combined perirhinal and postrhinal cortex lesions on object and place memory in the rat. J Neurosci 19:495-502.

Bzdok D, Yeo BTT (2017) Inference in the age of big data: future perspectives on neuroscience. Neuroimage 155:549-64.

Carpenter B, Gelman A, Hoffman MD, Lee D, Goodrich B, Betancourt M, Brubaker M, Guo J, Li P, Riddell A (2017) Stan: A probabilistic programming language. J Stat Softw 76:1-32.

Cholvin T, Loureiro M, Cassel R, Cosquer B, Geiger K, De Sa Nogueira D, Raingard H, Robelin L, Kelche C, Pereira de Vasconcelos A, Cassel JC (2013) The ventral midline thalamus contributes to strategy shifting in a memory task requiring both prefrontal cortical and hippocampal functions. J Neurosci 33:8772-83.

Clark RE, Zola SM, Squire LR (2000) Impaired recognition memory in rats after damage to the hippocampus. J Neurosci 20:8853-8860.

Darlington TR, Beck JM, Lisberger SG (2018) Neural implementation of Bayesian inference in a sensorimotor behavior. Nat Neurosci 21:1442-51.

Davoodi FG, Motamedi F, Naghdi N, Akbari E (2009) Effect of reversible inactivation of the reuniens nucleus on spatial learning and memory in rats using Morris water maze task. Behav Brain Res 198:130-135.

de Lima MN, Luft T, Roesler R, Schröder N (2006) Temporary inactivation reveals an essential role of the dorsal hippocampus in consolidation of object recognition memory. Neurosci Lett 405:142-146.

Dolleman-van der Weel MJ, Morris RG, Witter MP (2009) Neurotoxic lesions of the thalamic reuniens or mediodorsal nucleus in rats affect non-mnemonic aspects of watermaze learning. Brain Struct Funct 213:329-42.

Ennaceur A, Neave N, Aggleton JP (1996) Neurotoxic lesions of the perirhinal cortex do not mimic the behavioural effects of fornix transection in the rat. Behav Brain Res 80:9-25.

Friston KJ, Glaser DE, Henson RN, Kiebel S, Phillips C, Ashburner J (2002) Classical and Bayesian inference in neuroimaging: applications. Neuroimage 16:465-83.

Gershman SJ (2013) Bayesian Behavioral Data Analysis. In: Encyclopedia of Computational Neuroscience. Jaeger D, Jung R (Ed.). Springer.

Gomez-Shiavon M, Chen LF, West AE, Buchler NE (2017) BayFish: Bayesian inference of transcription dynamics from population snapshots of single-molecule RNA FISH in single cells. Genome Biol 18:164.

Hallock HL, Wang A, Shaw CL, Griffin AL (2013) Transient inactivation of the thalamic nucleus reuniens and rhomboid nucleus produces deficits of a working-memory dependent tactile-visual conditional discrimination task. Behav Neurosci 127:860-6.

Hannesson DK, Howland JG, Phillips AG (2004) Interaction between perirhinal and medial prefrontal cortex is required for temporal order but not recognition memory for objects in rats. J Neurosci 24:4596-604.

Hembrook JR, Mair RG (2011) Lesions of reuniens and rhomboid thalamic nuclei impair radial maze win-shift performance. Hippocampus 21:815-26.

Hembrook JR, Onos KD, Mair RG (2012) Inactivation of ventral midline thalamus produces selective spatial delayed conditional discrimination impairment in the rat. Hippocampus 22:853-860.

Ho JW, Narduzzo KE, Outram A, Tinsley CJ, Henley JM, Warburton EC, Brown MW (2011) Contributions of area Te2 to rat recognition memory. Learn Mem 18:493–501.

Hoover WB, Vertes RP (2012) Collateral projections from reuniens nucleus of thalamus to hippocampus and medial prefrontal cortex in the rat: a single and double retrograde fluorescent labelling study. Brain Struct Funct 217:191–209.

Kinnavane L, Amin E, Horne M, Aggleton JP (2014) Mapping parahippocampal systems for recognition and recency memory in the absence of the rat hippocampus. Eur J Neurosci 40:3720-34.

Kording KP (2014) Bayesian statistics: relevant for the brain? Curr Opin Neurobiol 25:150-3.

Kovács KJ (2008) Measurement of Immediate-Early Gene Activation – c-fos and Beyond. J Neuroendocrinol 20:665-72.

Layfield DM, Patel M, Hallock H, Griffin AL (2015) Inactivation of the nucleus reuniens/rhomboid causes a delay-dependent impairment of spatial working memory. Neurobiol Learn Mem 125:163-7.

Lopez J, Herbeaux K, Cosquer B, Engeln M, Muller C, Lazarus C, Kelche C, Bontempi B, Cassel JC, de Vasconcelos AP (2012) Context-dependent modulation of hippocampal and cortical recruitment during remote spatial memory retrieval. Hippocampus 22:827-41.

Loureiro M, Cholvin T, Lopez J, Merienne N, Latreche A, Cosquer B, Geiger K, Kelche C, Cassel JC, Pereira de Vasconcelos A (2012) The ventral midline thalamus (reuniens and rhomboid nuclei) contributes to the persistence of spatial memory in rats. J Neurosci 32:9947-59.

Mathiasen ML, Amin E, Nelson AJD, Dillingham CM, O'Mara SM, Aggleton JP (2019) Separate cortical and hippocampal cell populations target the rat nucleus reuniens and mammillary bodies. Eur J Neurosci. doi: 10.1111/ejn.14341. [Epub ahead of print]

McGuinness L, Taylor C, Taylor RDT, Yau C, Langenhan T, Hart ML, Christian H, Tynan PW, Donnelly P, Emptage NJ (2010) Presynaptic NMDARs in the hippocampus facilitate transmitter release at theta frequency. Neuron 68:1109-27.

McKenna JT, Vertes RP (2004) Afferent projections to nucleus reuniens of the thalamus. J Comp Neurol 480:115-42.

Mitchell JB, Laiacona J (1998) The medial frontal cortex and temporal memory: tests using spontaneous exploratory behaviour in the rat. Behav Brain Res 97:107-13.

Morgan JI, Cohen DR, Hempstead JL, Curran T (1987) Mapping patterns of c-fos expression in the central nervous system after seizure. Science 237:192–7.

Park M, Pillow JW (2011) Receptive field inference with localized priors. PLoS Comput Biol 7:e1002219.

Paxinos G, Watson C (2005) The rat brain in stereotaxic coordinates. Academic Press.

Prescott MJ, Lidster K (2017) Improving quality of science through better animal welfare: the NC3Rs strategy. Lab Anim 46:152-6.

Russell WMS, Burch RL (1959) The principles of humane experimental technique. Methuen.

Swanson LW (1998) Brain maps: structure of the rat brain. Elsevier.

Townsend JP, Hartl DL (2002) Bayesian analysis of gene expression levels: statistical quantification of relative mRNA levels across multiple strains or treatments. Genome Biol 3:research0071.1-16.

Van de Schoot, Depaoli S (2014) Bayesian analyses: where to start and what to report. J The European Health Psychologist 16:75-84.

Vertes RP (2002) Analysis of the projections from the medial prefrontal to the thalamus in the rat with emphasis on nucleus reuniens. J Comp Neurol 442:163-87.

Vertes RP, Hoover WB, DoValle AC, Sherman A, Rodriguez JJ (2006) Efferent projections of the reuniens and rhomboid nuclei of the thalamus in the rat. J Comp Neurol 499:768-96.

Viena TD, Linley SB, Vertes RP (2018) Inactivation of nucleus reuniens impairs spatial working memory and behavioral flexibility in the rat. Hippocampus doi: 10.1002/hipo.22831. [Epub ahead of print]

Wan H, Aggleton JP, Brown MW (1999) Different contributions of the hippocampus and perirhinal cortex to recognition memory. J Neurosci 19:1142-8.

Wickham H (2016) ggplot2: Elegant Graphics for Data Analysis. Springer-Verlag New York.

Winters BD, Forwood SE, Cowell RA, Saksida LM, Bussey TJ (2004) Double dissociation between the effects of peri-postrhinal cortex and hippocampal lesions on tests of object

recognition and spatial memory: heterogeneity of function within the temporal lobe. J Neurosci 24:5901-8.

Woolrich MW (2012) Bayesian inference in FMRI. Neuroimage 62:801-10.

Wouterlood FG, Saldana E, Witter MP (1990) Projection from the nucleus reuniens thalami to the hippocampal region: light and electron microscopic tracing study in the rat with the anterograde tracer Phaseolus vulgaris-leucoagglutinin. J Comp Neurol. 296:179–203.

Xu W, Sudhof TC (2013) A neural circuit for memory specificity and generalization. Science 339:1290-5.

Zhu XO, Brown MW, Aggleton JP (1995a) Neuronal signalling of information important to visual recognition memory in rat rhinal and neighbouring cortices. Eur J Neurosci. 7:753–65.

Zhu XO, Brown MW, McCabe BJ, Aggleton JP (1995b) Effects of the novelty or familiarity of visual stimuli on the expression of the immediate early gene c-fos in rat brain. Neuroscience 69:821-9.

Zhu XO, McCabe BJ, Aggleton JP, Brown MW (1996) Mapping visual recognition memory through expression of the immediate early gene c-fos. Neuroreport 7:1871-5.

List of Abbreviations

ABC	Avidin-biotinylated horseradish peroxidase complex
ACC	Anterior cingulate cortex
ANOVA	Analysis of variance
AP	Anterior-posterior
BSA	Bovine serum albumin
CA1-3	Cornu Ammonis 1-3
DAB	Diaminobenzidine
DCA1-3	Dorsal CA1-3
DDG	Dorsal dentate gryrus
ddH2O	Double distilled water
DG	Dentate gyrus
DMSO	Dimethyl sulfoxide
DPC	Dorsal peduncular cortex
DSUB	Dorsal subiculum
DV	Dorsal ventral
ICA1-3	Intermediate CA1-3
IDG	Intermediate dentate gyrus
IFC	Infralimbic cortex
LENT	Lateral entorhinal cortex
M2C	Motor cortex M2
MIA	Modular image analysis
ML	Mediolateral
MOC	Medial orbital cortex
NACWO	Named Animal Care and Welfare Officer

NMDA	N-methyl-D-aspartate
NHST	Null Hypothesis Significance Testing
NRe	Nucleus reuniens of the thalamus
NRh	Rhomboid nucleus of the thalamus
PB	Phosphate buffer
PBST	Phosphate buffered saline with Triton
PRH	Perirhinal cortex
PRL	Prelimbic cortex
PSTC	Postrhinal cortex
ROI	Region of interest
SD	Standard deviation
s.e.m.	Standard error of the mean
TE2	Temporal association cortex
V2C	Visual cortex V2
VCA1-3	Ventral CA1
VDG	Ventral dentate gyrus
VOC	Ventral orbital cortex
VSUB	Ventral subiculum
Weka	Waikato Environment for Knowledge Analysis

Appendix

Table A.1: Steps for dehydration and cresyl staining of microscope slides

Step	Solution	Time period
1.	70% Ethanol	3 - 5 min
2.	ddH2O	10 seconds
3.	Cresyl Stain	20 – 30 mins
4.	70% ethanol	Section specific (5 mins)
5.	100% ethanol	3 - 5 min
6.	100% ethanol	3 - 5 min
7.	Xylene	2 min
8.	Xylene	5 min

Figure A.1: Diagram of ROIs taken at 4.20 and 2.70mm relative to Bregma. Figure taken and adapted from Swanson atlas, 1998.

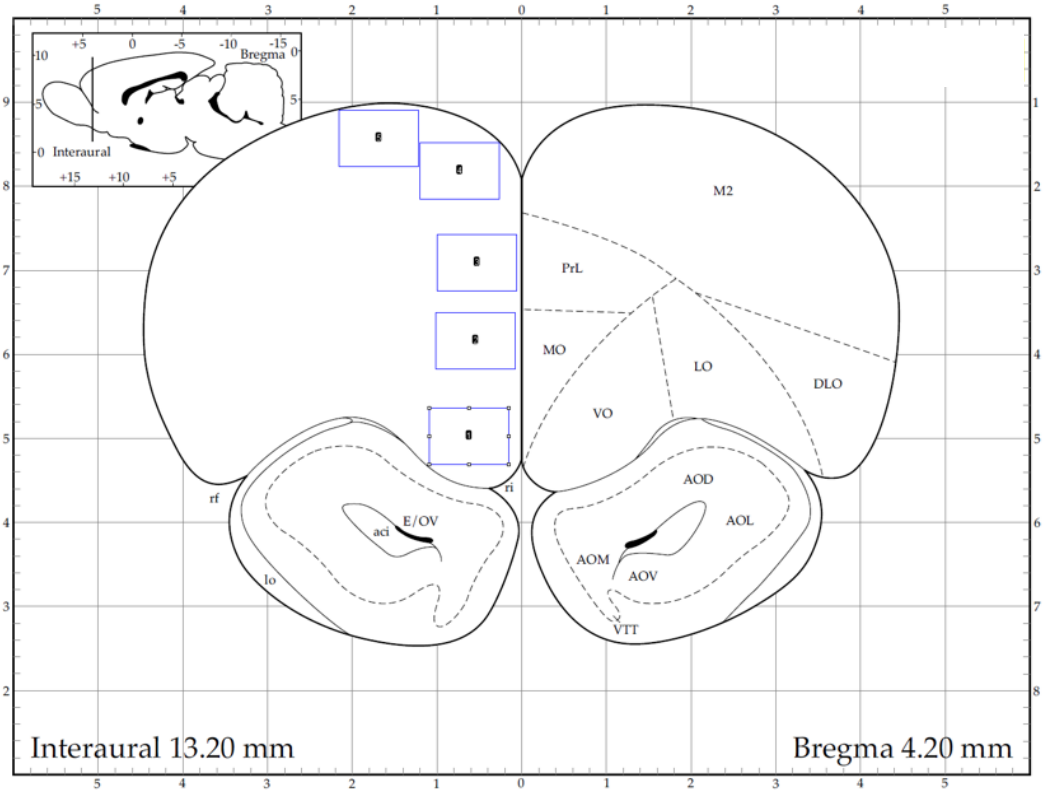

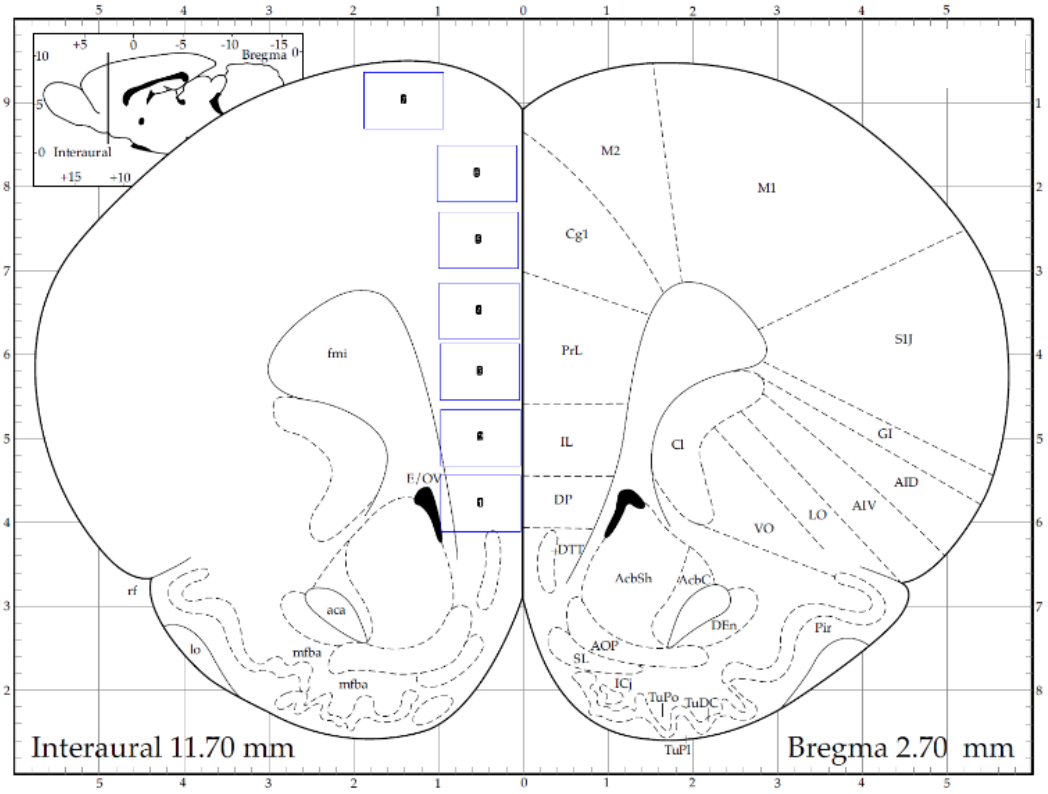

Figure A.2: Diagram of ROIs taken at -2.56 and -4.80mm relative to Bregma. Figure taken and adapted from Swanson atlas, 1998.

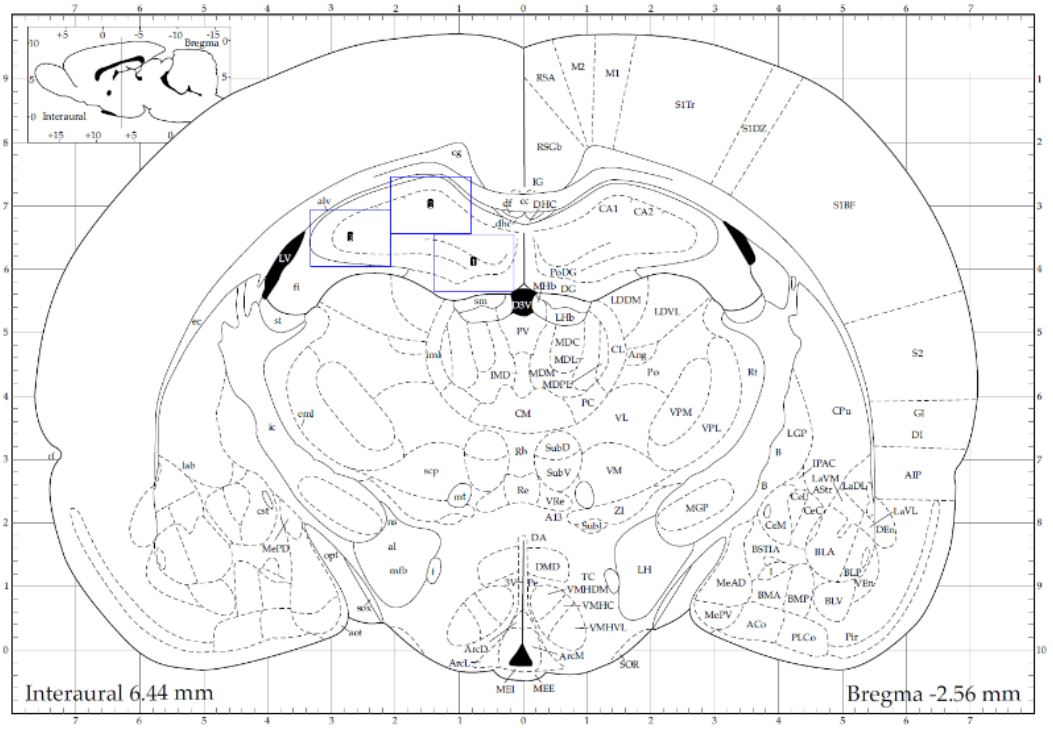

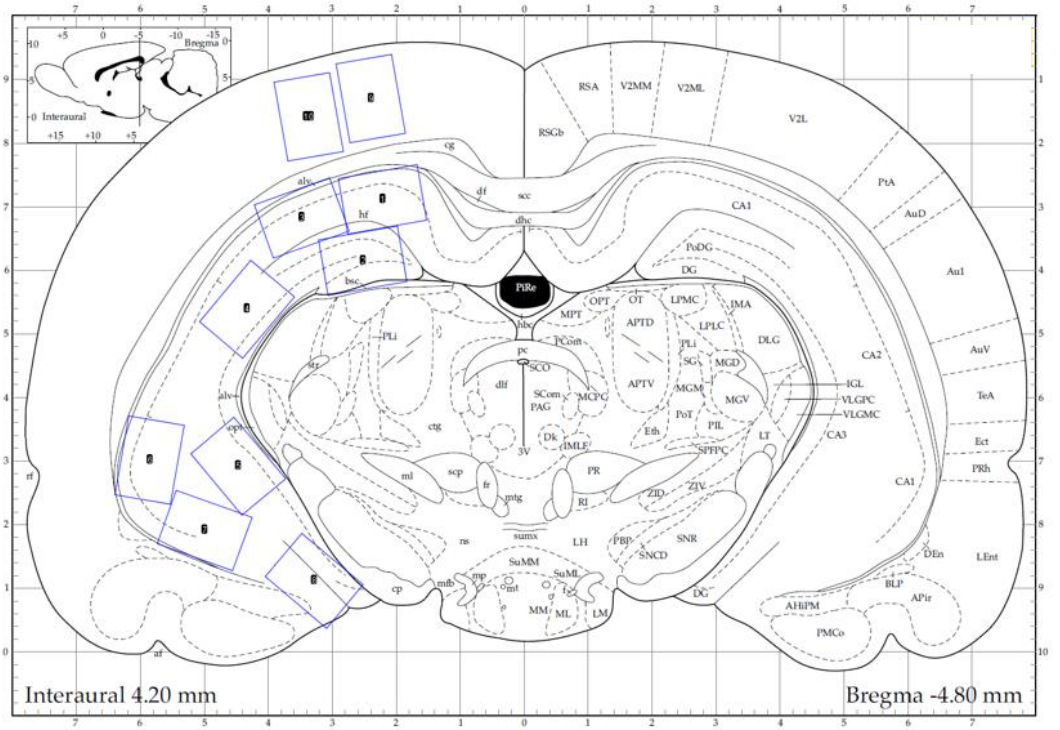

Figure A.3: Diagram of ROIs taken at -5.30 and -6.30mm relative to Bregma. Figure taken and adapted from Swanson atlas, 1998.

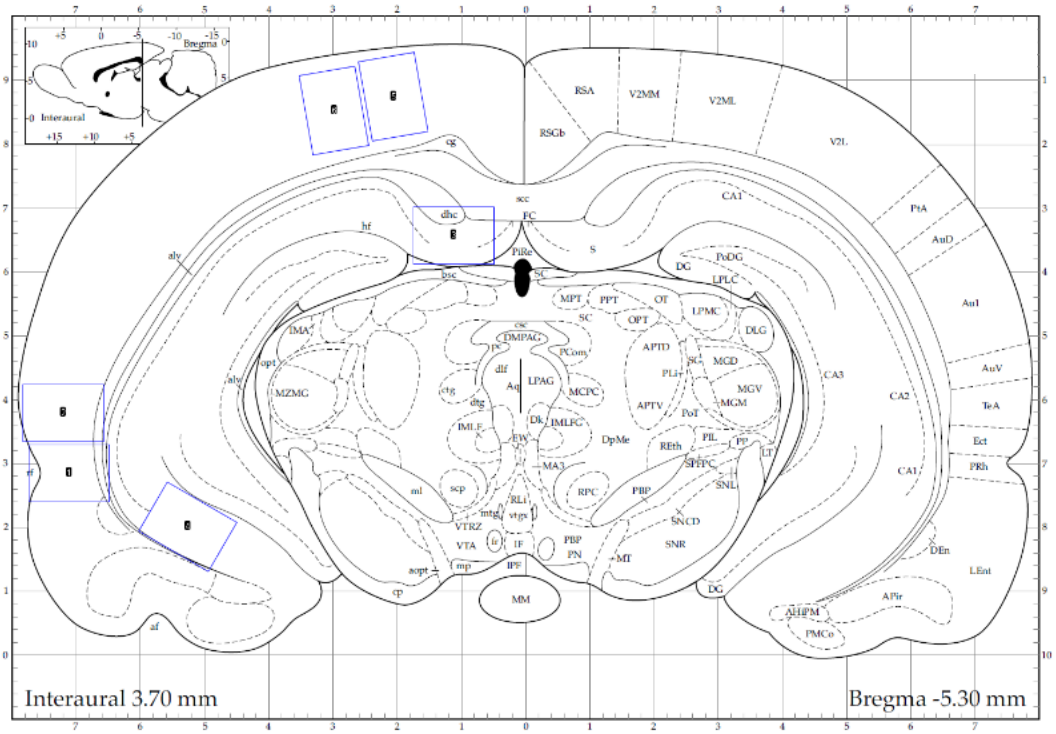

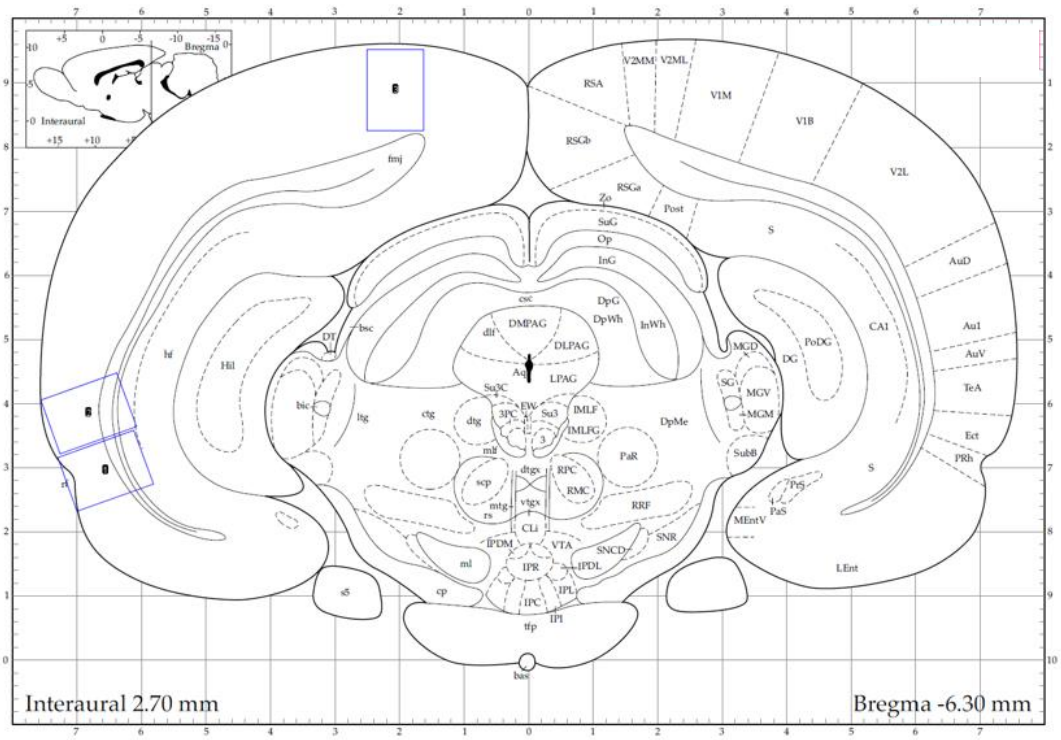

Figure A.4: Diagram of ROIs taken at -7.30 and -8.30 relative to Bregma. Figure taken and adapted from Swanson atlas, 1998.